DLR Design Challenge 2025

Adaptive **E**mergency **T**ransport for **H**umanitarian **E**vacuation & **R**esponse

Submitted July 21, 2025

Team Participants

Daniel Götz
Johannes Götzen
Raman Law
Laurin Piechotta (Teamleader)
Süheyl Savran
Carlos Santiago Valladares Q.

Academic Advisor

Prof. Dr.-Ing. Carsten Braun

Team Members

Daniel Götz
M. Sc.
Aerospace Engineering
2nd Semester

Johannes Götzen
B. Eng.
Aerospace Engineering
18th Semester

Raman Law
M. Sc.
Aerospace Engineering
3rd Semester

Laurin Piechotta
M. Sc.
Aerospace Engineering
1st Semester

Süheyl Savran
M. Sc.
Aerospace Engineering
1st Semester

Santiago Valladares
M. Sc.
Aerospace Engineering
1st Semester

Abstract

The **A**daptive **E**mergency **T**ransport for **H**umanitarian **E**vacuation & **R**esponse (AETHER) is a rescue aircraft for 19 passengers. Key design feature is the versatility derived from different scenarios. The concept includes a convertible cabin layout, a rear loading concept, a pressurized cabin, and a two-engine layout with Sustainable Aviation Fuel as an energy source.

Three different rescue missions were considered to optimize the aircraft for each scenario. In a comparative study similar sized airplanes were used to determine current state of the art development and as a starting point for improvements.

Zusammenfassung

Das Flugzeug **A**daptive **E**mergency **T**ransport for **H**umanitarian **E**vacuation & **R**esponse (AETHER) ist ein Rettungsflieger für 19 Passagiere. Hautmerkmal des Konzepts ist die Variabilität, die sich aus den verschiedenen Szenarien ergibt. Es umfasst eine umrüstbaren Kabineninnenraum, eine Beladekonzept von hinten, eine Druckkabine und einen zweimotorigen Antrieb, der mit nachhaltigem Flugkraftstoff betrieben werden kann.

Es wurden drei verschiedene Rettungsszenarien berücksichtigt, um das Flugzeug auf jedes einzelne hin zu optimieren. In einer Vergleichsstudie wurden Flugzeuge ähnlicher Größe verwendet, um den aktuellen Stand der Entwicklung zu ermitteln und als Ausgangspunkt für Verbesserungen zu nutzen.

Approval Letter

FH AACHEN
UNIVERSITY OF APPLIED SCIENCES

CONFIRMATION OF SUBMISSION

I hereby confirm that the contribution submitted by the student team from the University of Applied Sciences in Aachen participating in the DLR Design Challenge 2025 has been reviewed and approved by me as a member of the university's academic staff.

The work presented reflects the team's own effort and has been carried out in accordance with academic standards. I fully endorse the team's participation in the competition and support the submission of their concept to the German Aerospace Center (DLR).

Team Members:

Süheyl Savran

Laurin Piechotta

C. Santiago Valladares Q.

Daniel Götz

Raman Law

Johannes Götzen

Aachen, 21.07.25
Place, Date

Prof. Dr.-Ing. Carsten Braun

Contents

List of Figures

List of Tables

1. Introduction

In recent years European countries have increased their annual defense expenditure allocation in response to political instability in neighboring states, driving up budgets by 17 per cent to USD 693 billion in 2024. [1]This intensification of military preparedness heightens awareness of escalations on European soil, with conflict naturally comes a parallel surge in demand for medical evacuation and emergency response. Unfortunately, in parallel the number of hospitals in Germany has declined over recent years as seen on [2], resulting in increased travel distances to specialized treatment centers.

These needs are further underscored by the operational challenges in remote regions, disaster-stricken areas, and densely populated urban centers plagued by ground-traffic congestion, all of which demand faster response times and greater operational flexibility.

Given the operational limitations of rotary-wing air ambulances, particularly their restricted range and cruise speed, fixed-wing aircraft are emerging as the preferred means of medical transport that should offer the same level of demand of steep approaches, STOL distances and operations on demanding surfaces and atmospheric conditions that would render many critical locations inaccessible with available solutions.

As clinical and logistical demands continue to grow, this opens the market for the development of a new generation of dedicated rescue aircraft that offer rapid, efficient, and safe air-transport solutions that integrate advanced medical systems with cutting-edge aviation technologies capable of accommodating increasingly complex and geographically dispersed emergency scenarios.

Enhanced range capabilities will not only facilitate patient repatriation and international transfers but also expand the potential catchment area for critical care services. Consequently, a broader population will gain timely access to advanced medical interventions, while operators benefit from an enlarged service market.

In the present study, we propose the conceptual design of a next-generation medical rescue aircraft, evaluated against a series of representative mission profiles to demonstrate its ability to meet these diverse clinical requirements and operational constraints.

2. Literature Review

Meeting the 2035 entry-into-service target with a fixed-wing MedEvac concept that marries conventional turboprop propulsion, 100 % sustainable aviation fuel (SAF) capability and a more-electric system architecture is fully supported by current research trajectories. Lifecycle and engine-bench data show that SAFs, especially Fischer-Tropsch and HEFA pathways, cut life-cycle CO_2 by 41–89 % and slash SO_2 and particulate emissions by up to 95 % without hardware changes, while recent turboprop combustion trials confirm that the thermal-NO_x signature remains within CS-25 limits. These findings substantiate the choice of a Pratt & Whitney-class twin turboprop configured for 100% SAF from day one.

High-wing aerodynamics with double-slotted Fowler flaps and leading-edge slats can be further leveraged by propeller slipstream. Wind-tunnel studies on propeller-wing-flap systems demonstrate that immersion of the flap in the slipstream lifts trimmed $C_{L,max}$ to around 3.0 and trims balanced field length by more than 25% relative to classical high-lift devices, performance that directly underpins sub-800 m operations on unpaved or icy strips envisioned for the MedEvac role [3].

Cabin layout can rely on the quick-change paradigms validated during the COVID-19 pandemic: pressurized isolation pods and modular life-support racks mounted onto standard litter tracks enabled fixed-wing ambulances to move ventilated patients over 25,000ft flight sectors with thirty-minute turn-rounds and no adverse clinical outcomes [4]. A rear ramp door is structurally compatible with CS-25 load cases and offers unobstructed, ground-level access for stretchers and bulky equipment.

Moving to more-electric secondary systems aligns naturally with SAF-optimized turboprops. The MEA reviews and experimental power-hardware demonstrators predict that by 2030-35, high-speed permanent-magnet generators and SiC inverters will support 270 VDC or ± 540 V architectures at power densities above 20 kW/kg, allowing electrically driven ECS packs, de-icing and actuation while the APU supplies gate-to-gate ground power. Such systems cut bleed-air extraction, improving specific fuel consumption and freeing thermal margin in the turboprop cycle, an important gain when operating in hot-and-high or cold crisis zones [5].

A collective analysis of these literature strands substantiates that each technological enhancement within the contemporary conservative configuration, namely 100% SAF turboprops, prop-blown double-slotted flaps, modular medical interiors, rear ramp loading, and MEA subsystems, will attain Technology Readiness Level (TRL) 7-8 prior to the year 2035. The design, therefore, achieves a robust balance between technical feasibility, operational flexibility on sub-800m rough fields, a 1,250km radius of action, and the rapid clinical turnarounds demanded of next-generation aeromedical evacuation.

3. Design requirements

To meet the given mission requirements and ensure high operational flexibility, the severity of specific mission parameters is ranked and given in the following web plot:

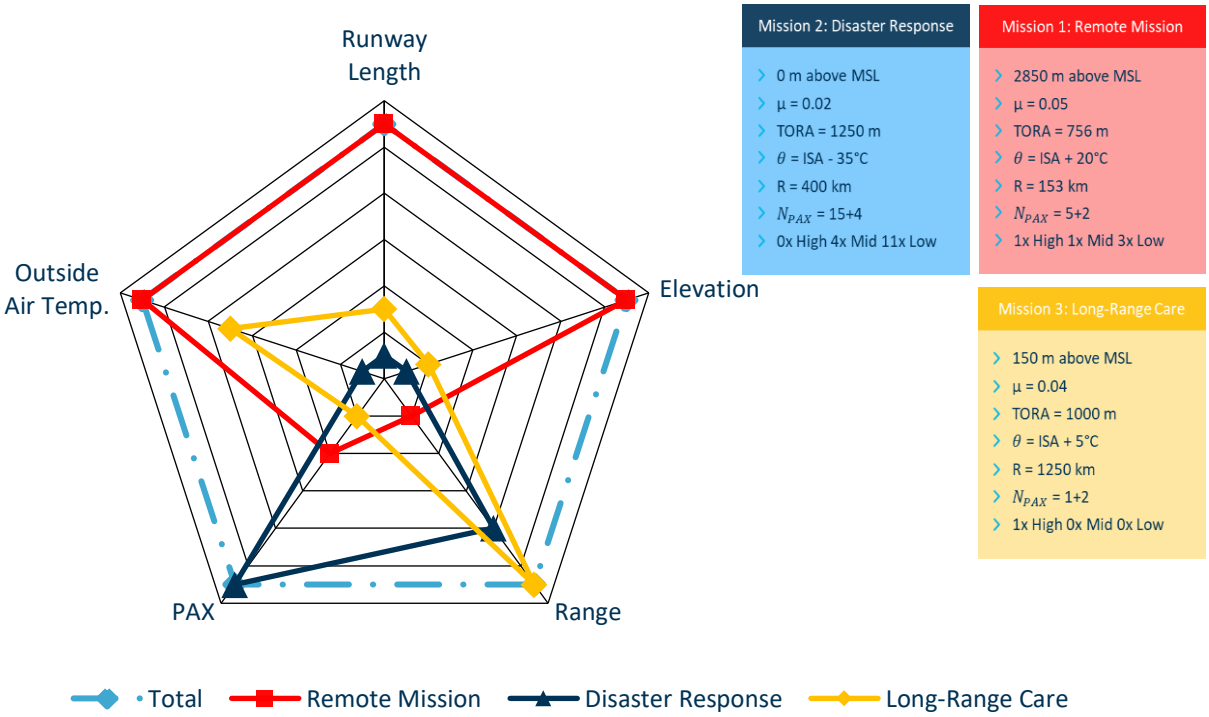

Figure 3-1 DLR Mission Requirements

The parameter set that is utilized for preliminary sizing is the combination of the shown parameters. The parameters of Mission 1 encompass air temperature, runway length and elevation. The parameters of Mission 2 comprise the payload, while Mission 3 defines the range. A comparative study has been conducted to initialize first values to calculate the required Power to Weight Ratio P/W and the required Wing Loading W/S. Comparing different regional turboprop aircraft the following values can be obtained:

$$C_{L,max} = 1.50 \left(C_{L,max,TO} = 2.00, C_{L,max,L} = 3.00\right),$$
$$\Lambda = 9, C_{D0} = 0.0312, L/D_{max} = 13.46, L/D_{max,TO} = 9.91, L/D_{max,L} = 6.33$$

This leads to the following matching diagram (Figure 3-2), which is a combined plot of three different matching diagrams based on three different requirements sets. The optimum design point is the highest minimum extremum, which is highlighted in the following:

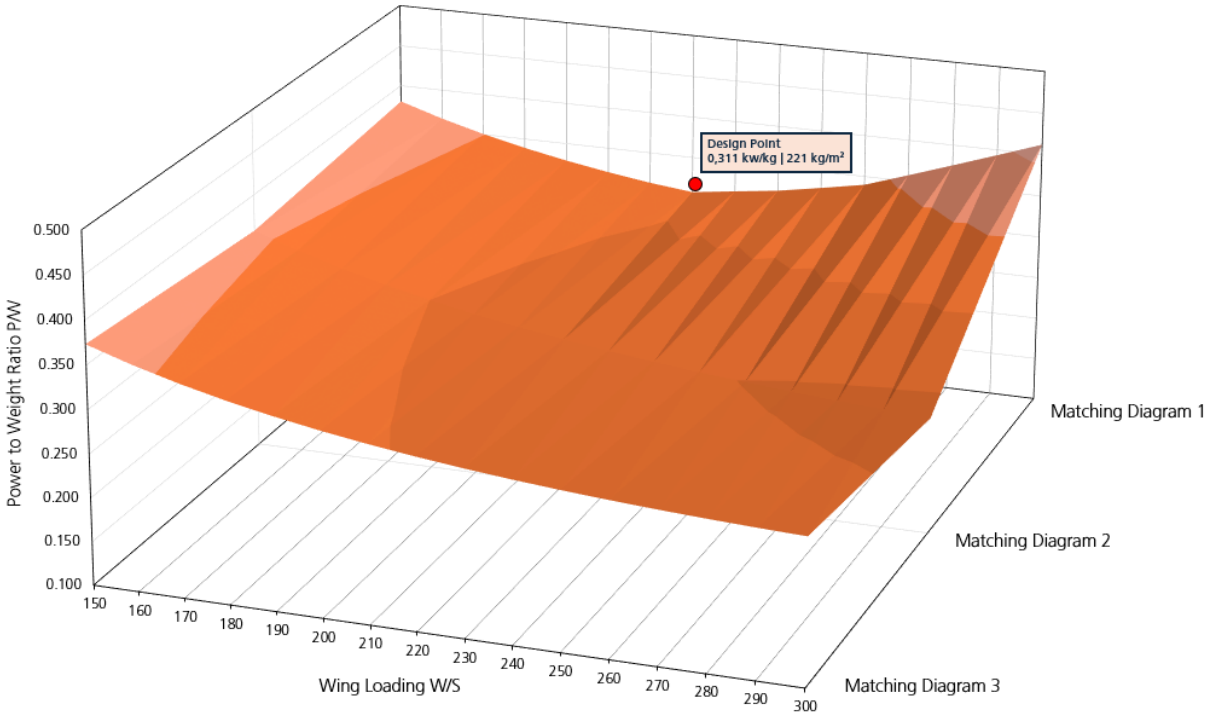

Figure 3-2 Combined Matching Diagram

4. Aircraft Concept

4.1 Fuselage

The primary function of the fuselage is to house the pressurized cabin and to serve as the structural backbone, interconnecting all major aircraft systems and subsystems. Under our TLAR, the fuselage geometry was driven by the volumetric needs of the second mission profile, "Humanitarian Response," which demands accommodation for 19 passengers, including four patients on medical stretchers. Although cabin layout specifics will be addressed in the dedicated section, it is important to note here that those requirements directly determined both the cabin and therefore fuselage length and overall external shape.

An initial fuselage length was estimated using a standard empirical approximation [6]:

$$L = a \cdot MTOM^{\,c} = 0.169 \cdot 1400^{0.51} = 22m$$

Where the statistical values a and c were chosen according to AETHER's twin turboprop category. Roskam's empirical statistics were then applied to establish an initial fineness ratio and to apportion length among cockpit, cabin, and tail cone sub-sections [7].

Given that AETHER cruises at 7620m and driven by potential passenger's medical conditions, the aircraft calls for pressurization. For this reason, a circular cross -section was adopted owing to its superior structural efficiency under internal pressure, uniform stress distribution, and straightforward manufacturing and inspection. Following integration of the most demanding mission scenario- volumetric layout, this configuration was refined to maximize usable interior volume and enhance occupant comfort, drawing inspiration from comparable platforms in this category. An outer diameter of 2.50 m, an inner cabin diameter of 2.30 m, a total fuselage length of 21.0 m, and a fineness ratio of 8.40, which balances aerodynamic drag and structural weight considerations. These dimensions are seen on the figures Figure 4-2 to Figure 4-4 below.

4.1.1 Cabin layout

After iterating different arrangements of seats, stretchers, medical equipment and their storage, a 2-abreast seating configuration was chosen. For a more efficient use of volume, the seats are facing inward. Another positive influence is that the doctors can see their patients face to face. Changed medical conditions can so be recognized in a faster way than in traditional seating where everyone is facing forward. Nevertheless, AETHER offers high modularity and therefore it is not limited to this seating configuration and the seat orientation can be easily adjusted to rotate 180 degrees to provide independent comfort to patients depending on their health situation and accessibility to the med crew to provide easier assistance.

Figure 4-1 - Rendering of the cabin's interior design

A key design requirement was accommodating medium- and severely injured patients on medical stretchers in compliance with DIN EN 13718-2 [8], which specifies the minimum clearances necessary for in-flight medical operations. The volumetric demands of these stretchers, combined with regulatory spacing requirements, necessitated an increase in cabin length. Various configurations were evaluated including vertical stacking of stretchers to conserve floor area, but this approach would have mandated a greater cabin height, yielding a larger fuselage diameter and a corresponding penalty in aerodynamic drag.

After a comprehensive assessment of aerodynamic performance, structural weight, and patient comfort, the final layout positions stretchers in single file rows along each side of the cabin. Locating these rows adjacent to the aft service door optimizes patient loading and unloading procedures, minimizes turnaround time for high acuity cases, and facilitates rapid deployment of bulky medical equipment. This side-by-side arrangement satisfies all clearance mandates while preserving efficient fuselage geometry and maintaining favorable drag characteristics.

The aircraft TLAR encompasses three distinct mission profiles with widely varying passenger counts, necessitating a reconfigurable cabin architecture to address diverse operational demands.

Modular interior layouts enable optimization of the aircraft's operational empty weight and payload distribution, thereby improving fuel efficiency and extending mission range. However, reconfiguration time poses an operational drawback; accordingly, rapid deployment of attachment system is essential. A review of existing solutions identified both: pinrail mechanisms and quick release studs with integrated locking features as viable technologies already in use.

For the floor mounting infrastructure, this design adopts the aviation certified Standard Airline Track (SAE AS33601 [9]) system. Its flush integration into the cabin floor allows seamless transitions between configurations while providing robust loadbearing capacity for seats, cargo pallets, medical stretchers, and ancillary equipment. The system's standardized interface ensures compatibility with off-the-shelf components, simplifies maintenance procedures, and supports rapid turnaround between missions—all critical for maximizing aircraft availability across varied humanitarian, medical evacuation, and passenger transport scenarios.

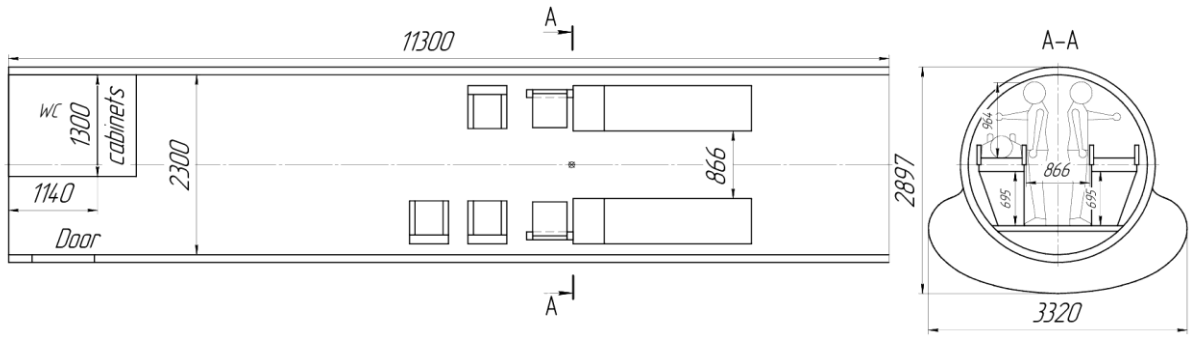

Figure 4-2: Cabin layout for scenario 1

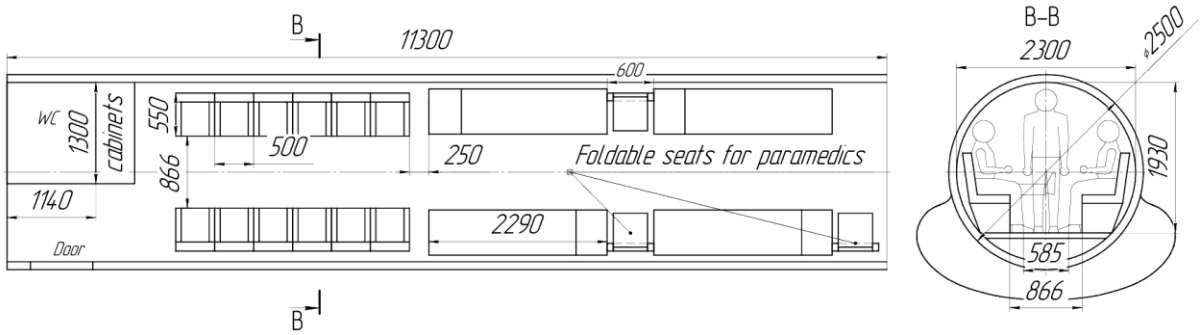

Figure 4-3: Cabin layout for scenario 2

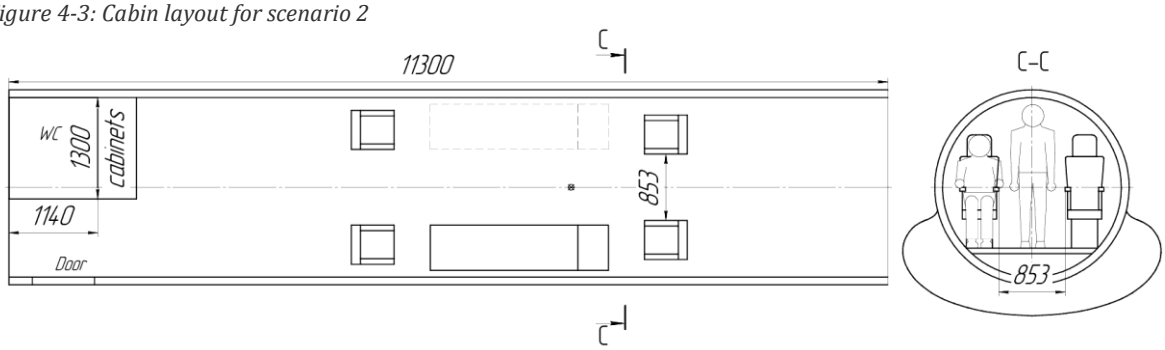

Figure 4-4: Cabin layout for scenario 3

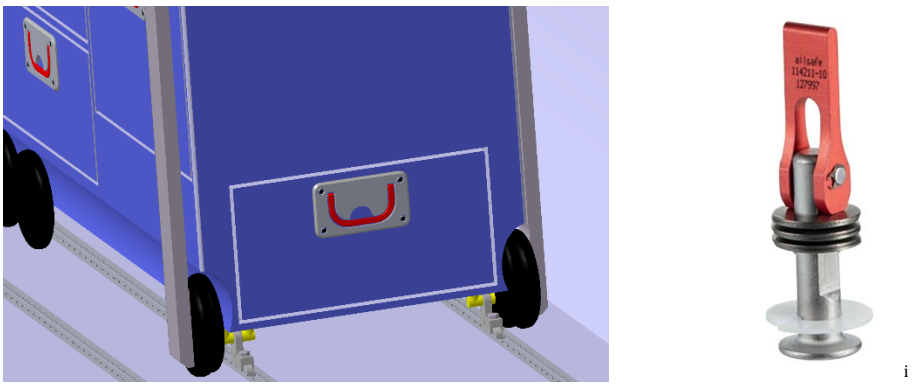

Figure 4-5: Quick Release Stud used to secure modular units.

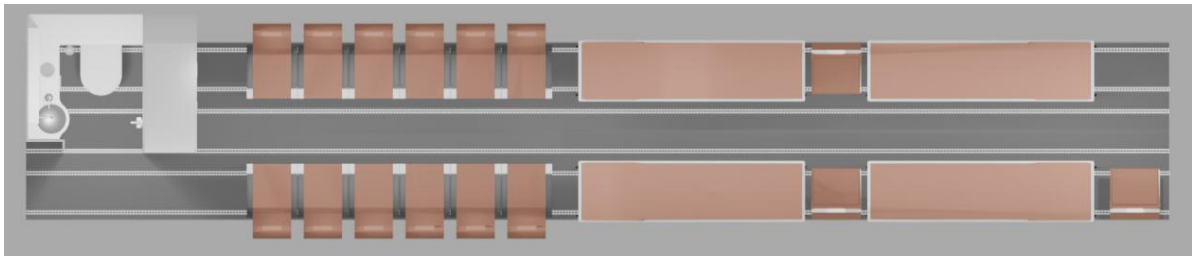

Figure 4-6: Rendered top view of cabin layout for Mission 2

4.1.2 Cockpit

AETHER's crew must maintain full operational capability under demanding conditions, the cockpit layout has been optimized to maximize situational awareness. The FOV extends approximately 90° to each side and 17° downward, enabling rapid detection of potential hazards and providing pilots with sufficient time to respond. Critical flight information is projected directly into the pilot's line of sight via a heads-up display (HUD), minimizing the need for large head movements and ensuring that essential data remain continuously visible.

Given AETHER's potential use in parallel to electronic-warfare environments, a fly-by-light (FBL) flight-control system has been selected over conventional FBW. Optical transmission is inherently immune to electromagnetic interference, preserving control integrity in contested areas where traditional electrical signaling could be a compromise.

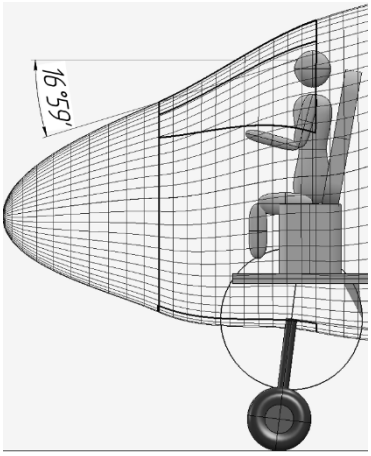

Figure 4-7: Over-nose view angle from the cockpit

4.1.3 Door arrangement

A further important part of the rescue aircraft is the door for the high injured people. First it must be decided whether a side door or a back door is sufficient. Patients with highly injuries must be moved as carefully as possible. This requirement leads to the suggestion of using a back door arrangement.

It must be as wide as possible to provide a safe walking area when injured patients get loaded and unloaded. Also, the inclination angle must be small. This helps when rolling the equipment in and out. The AETHER backdoor has a width of 1.9m and an inclination angle of 12°. The vertical height from the walking area to the fuselage is minimum 1.9m. A positive aspect of this construction is the possibility to make the outer skin rounded. Other aircraft with a backdoor have a flat outer skin to provide an even laying on the ground. AETHER can be shaped more aerodynamically since turbulence can be avoided. Figure 4 8: Side View of opened back door In front of the fuselage a side door is placed. The board the opened be subdivided into two groups. The patients with slight injuries can use the front side door and people with medium/ high injuries can use the back door. This helps to improve the boarding time. A further advantage is that there are more emergency exits. Which helps the chances of surviving in case of a crash. It should include a discussion of the design requirements derived, including all requirements derived for subsystems.

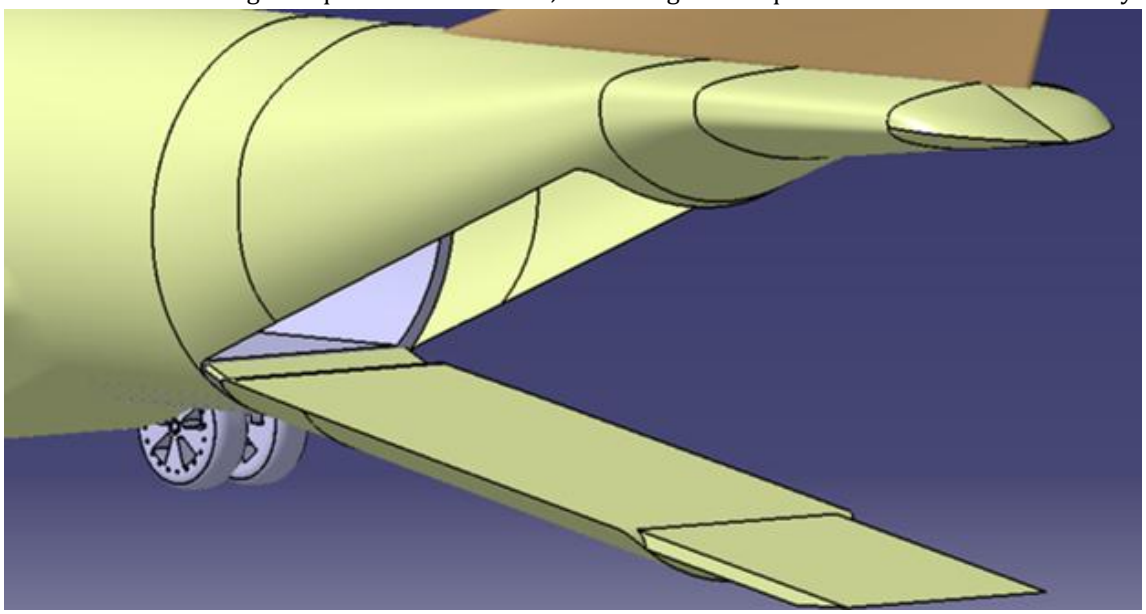

Figure 4-8 : Rear back door arrangement

4.2 Wing Aerodynamics

4.2.1 Wing Planform and Airfoil Selection

AETHER features a high-mounted wing with a span of $b \approx 24$m and an aspect ratio of AR=9, optimized to balance extreme STOL needs with cruise efficiency. A high wing was chosen using a decision matrix, to improve low-speed stability, good ground accessibility for the paramedics and ground clearance for the wing-mounted turboprop engines. Furthermore, it benefits from the prop-blown slipstream over the wing and flaps increases C_L and $C_{L,max}$, cutting both take-off roll and approach speed, essential for the 756m TOFL / LFL requirement.

The wing has no quarter-chord sweep (Λ_{25} = 0°) to maximize lift at take-off (sweep generally reduces $C_{L,max}$) and a moderate taper ratio of λ = 0.5 to approach an elliptical lift distribution while reducing wing structural weight. The reference area $S_{ref} = 63.35m^2$ yields a wing loading of $W/S \approx 221\ kg/m^2$ at $MTOM = 14{,}000\ kg$, which fulfills the predefined design point (Figure 3-2). Thus, the airfoil and high-lift devices are tailored to achieve a large $C_{L,max}$ under "hot-and-high" conditions (takeoff altitude 2,850m, ISA+20 °C). A slight aerodynamic twist of -2° is incorporated (washout), so the wing tip operates at a lower angle of attack than the root. This helps ensure the inboard wing (near the fuselage) stalls before the outboard sections, maintaining aileron control at the stall. No geometric dihedral (v=0°) is used, as the high-wing configuration already provides lateral stability through the dihedral effect [10].

The wing employs a NACA 65_2-415 airfoil (15% thickness-to-chord) along most of the span. The tip contains a NACA 65_2-412 airfoil, which provides a higher $C_{L,max}$ and therefore counters a tip stall [11]. These are laminar-flow airfoils from the NACA 6-series, chosen for its low drag "bucket" ($C_{d,min}$ = 0.004) at cruise design lift coefficients ($C_l \approx 0.2$ to 0.8) [11]. The design lift coefficient of 0.4 corresponds to the airfoil's low-drag bucket, supporting efficient cruise at 136 m/s (M = 0.42). The airfoil's thickness (15%) provides volume for structure, fuel and high-lift mechanisms and yields a gentler stall behavior than very thin sections [12]. In flow conditions of Re≈$9*10^6$ it can attain a $c_{L,max} \approx 1.62$ at around α_{max}=16° [12]. The wing is inclined with a 2.8° incidence to the fuselage reference line. This is done to achieve the estimated $C_{L,cruise}$ = 0.4 at cruise flight for an angle of attack of α = 0°. By canting the wing at the same angle, the body attitude in level flight remains near 0°, minimizing fuselage and pylons' form drag, keeping the cabin floor level for medical equipment, and preserving cockpit visibility. The incidence therefore complements the -2° wash-out. The root chord operates at an effective +0.8° during cruise while the tips remain slightly negative, delaying tip stall and reducing trim drag at low-speed, high-lift settings. The estimation of the clean wing aerodynamic performance is done by using VSPaero, a software by NASA. The following results can be obtained by using a Vortex Lattice Method to calculate numerically the lift curve 4-9 and spanwise lift coefficient distribution Figure 4-10.

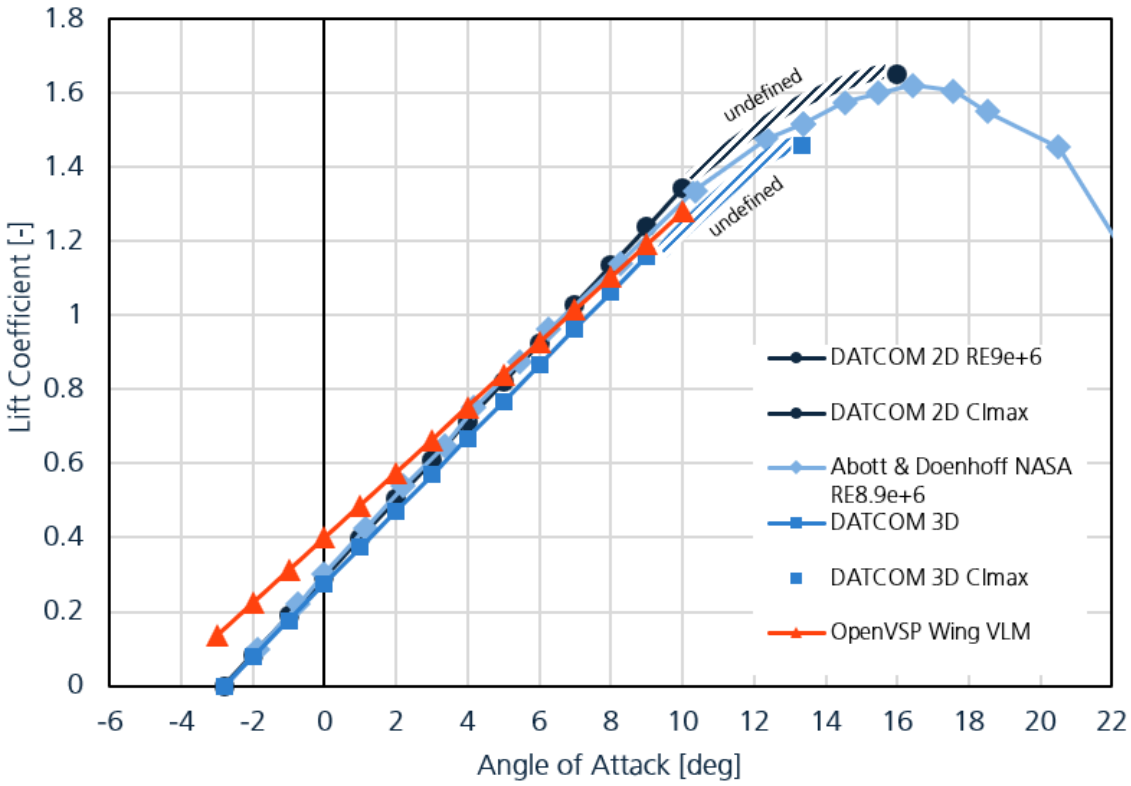

Figure 4-9 Lift Coefficient over angle of attack

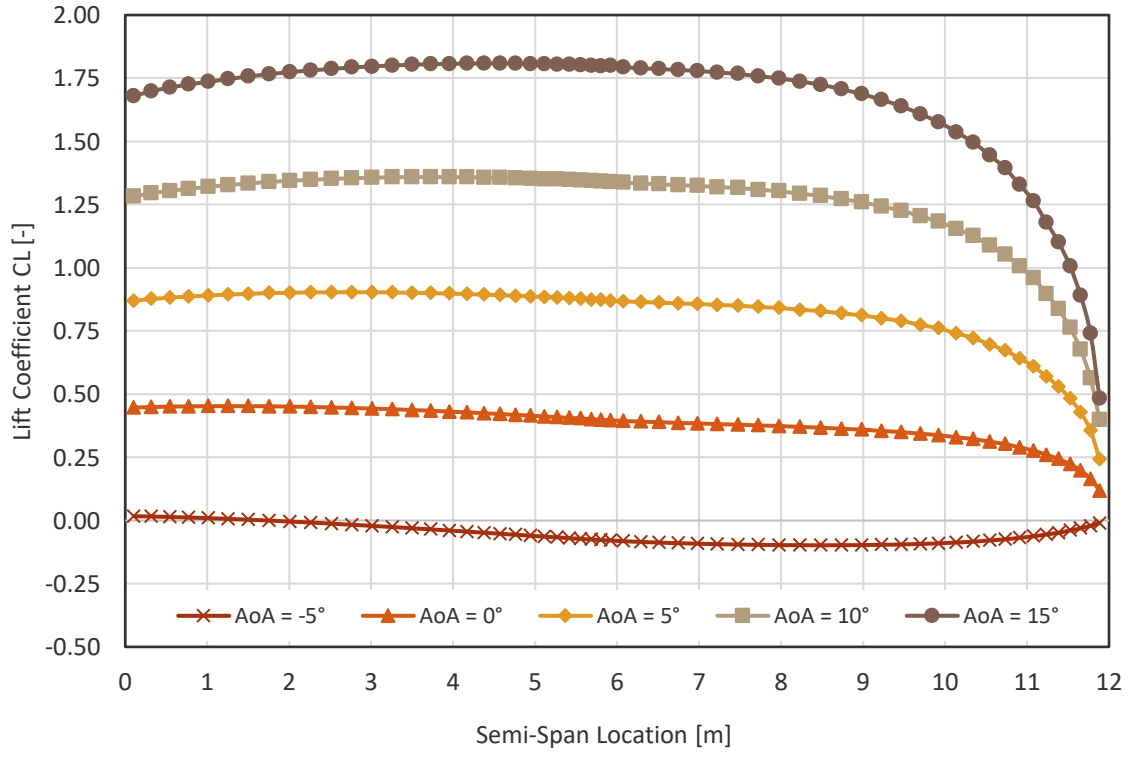

Figure 4-10 Lift distribution spanwise

4.2.2 High Lift Devices

To satisfy the stringent STOL criteria (s_{TOFL} & s_{LFL} < 756 m at "Hot-High"), the wing has been equipped with high-performance multi-element high-lift devices. A double-slotted fowler flap system spans about 53% of the wing (inboard) and has a large flap chord ratio of c_f/c = 0.35. In landing configuration, the flaps deflect at δ_f =45° (20° at take-off), substantially increasing camber and wing area. Leading-edge slats cover ~77% of the span, with a slat chord ratio of c_S/c = 0.20 and a deflection of δ_s =30° (10° at take-off). This combination is designed to roughly double the wing's lift coefficient compared to the clean wing. The double-slotted fowler flaps increase lift by both camber and chord extension. Such flaps can yield $\Delta C_{l,max,f}$ on the order of 1.5 - 2.0 (per airfoil) in landing deflection [6]. The slats energize the boundary layer over the wing's front, allowing the wing to sustain higher angles of attack. A slat typically adds about $\Delta C_{l,max,S} \approx 0.5 - 0.8$ (per airfoil) [6]. In combination, these devices are expected to increase the wing's $C_{L,max}$ ≈1.5 (clean 3D value) to above 3.0 [6].

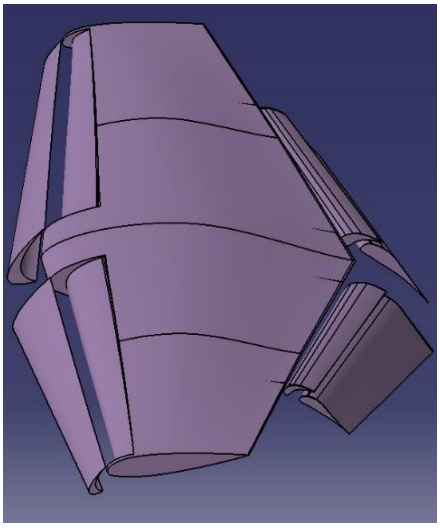

Figure 4-9: High Lift Devices CAD Design

The estimation of the wing's performance in high-lift configuration relies on semi-empirical methods (specifically, the USAF DATCOM methodology [13]) rather than direct simulation, because advanced high-lift devices have complex aerodynamic behavior which cannot be captured precisely through VSPaero. Using DATCOM correlations [13], the additional lift from deploying the flaps and slats was calculated and then added to the clean-wing baseline:

$$\Delta C_{L,max,f} = k_1 k_2 k_3 (\Delta C_{l,max})_{base} * \frac{S_{W_f}}{S_W} * K_\Lambda = 1.10\ (0.34\ for\ TO)$$

$$\Delta C_{L,max,S} = \left(\frac{\partial c_l}{\partial \delta_S}\right)_{max} \eta_{max} \eta_\delta \delta_S * \frac{c'}{c} * \frac{S_{W_f}}{S_W} = 0.724\ (0.42\ for\ TO)$$

With the estimated values for the $C_{L,max}$ of the clean wing and the additional values based on DATCOM, a $C_{L,max,L}$ and $C_{L,max,TO}$ can be achieved of:

$$C_{L,max,L} = C_{L,max} + \Delta C_{L,max,f,L} + \Delta C_{L,max,S,L} = 3.33$$

$$C_{L,max,TO} = C_{L,max} + \Delta C_{L,max,f,TO} + \Delta C_{L,max,S,TO} = 2.26$$

Beyond passive flaps and slats, the design leverages a propeller-blown wing to generate powered lift during take-off. At take-off thrust each propeller with a diameter of 3.4 m accelerates the airflow over the wing area behind the propeller (~30% of the wing area). To validate the effect on the lift coefficient a 2D approximation is used. The dynamic pressure in the propeller slipstream rises with the square of velocity, which is proportional to the local lift coefficient increase, stated by following equation [3]:

$$C_{L,blown} = C_{L,unblown} * \left(\frac{V_{jet}}{V_\infty}\right)^2$$

$$\left(\frac{V_{jet}}{V_\infty}\right)^2 = 1 + \frac{T}{0.5 * \rho * V_\infty^2 * A_{jet}}$$

This equation is only valid for take-off and landing, where the total thrust T of the blown wing is fixed and the jet velocity V_{jet} is fixed by the jet area A_{jet} [3].

The quantification of the exact increase in lift coefficient due to propeller slipstream is quite complex for a finite 3D wing. Based on wind tunnel data and CFD analysis shown in **Error! Reference source not found.**, it can be stated that the maximum local lift coefficient can be increased by 1 to 1.5, so for our configuration, where the propeller slipstream covers approximately 30% of the wing area, it would have roughly an increase of $\Delta C_{L,blown} \approx 0.3$ to 0.45. Because this value is not precisely validated the overall A/C performance in chapter 5 during take-off and landing will be evaluated only for the high-lift devices.

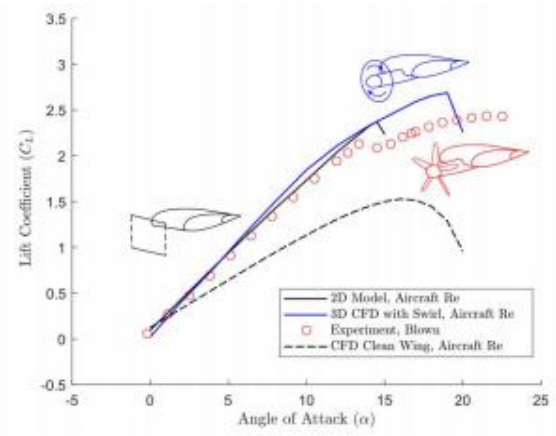

Figure 4-10 - Slipstream effect on blown wing [3]

4.2.3 Spoiler and Aileron Placement

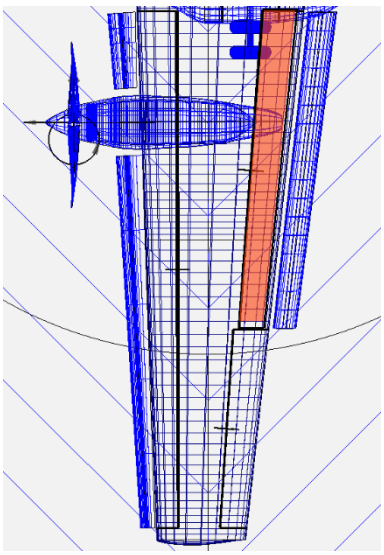

Figure 4-11: Spoiler Positioning

The aircraft is equipped with a flap span ratio of 53%, which means that nearly half of the wing´s span is covered with double slotted fowler flaps. The rest is covered with the aileron device with the span ratio of 35% and a chord ratio of 30%. The size requires a detailed analysis of the flight mechanical behavior which extends the conceptual design.

AETHER is designed for STOL applications and thus for steep flight paths in mountainous regions, especially in the mission 1 scenario. Therefore, spoilers are needed to reduce lift on ground, increase drag in approach and can enhance the roll mechanics by differential deflection. The span location is fixed with the flap positioning and the chordwise ending at 95%. This allows the placement of the actuator on the rear spar of the wing box.

4.2.4 Load & Structure Concept

Wing Load

The load, which is expected, must be estimated. In a horizontal unaccelerated flight (n=1) the loads acting on the wing are the lift (spanwise distributed), tank mass, wing mass and engine group mass. To calculate the normal force, the wing is divided into finite elements via MATLAB and the different load inputs are applied (masses can be extracted on Table 5-1). Leading to the following distributions:

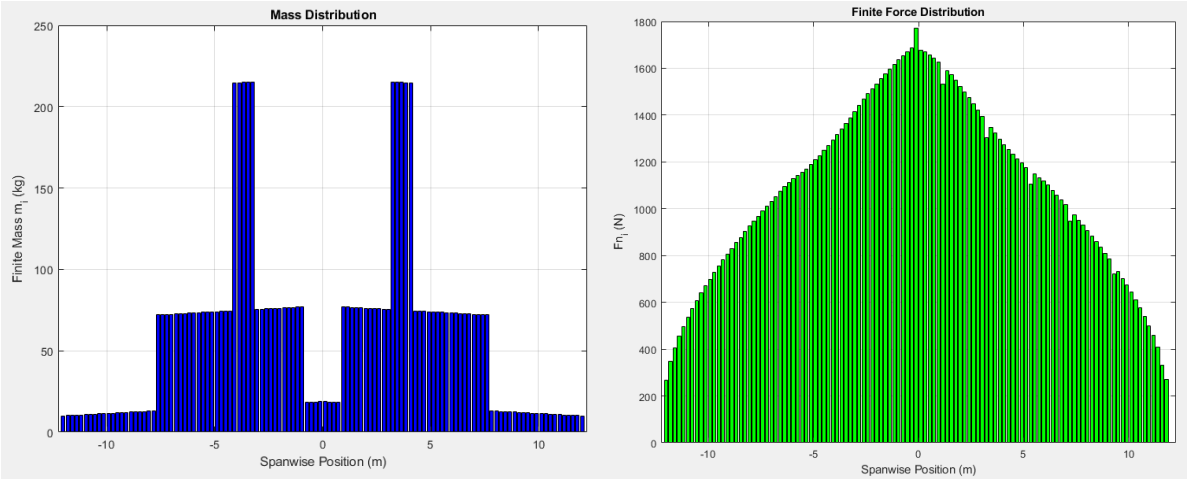

Figure 4-12: Finite Mass & Load Distribution from MATLAB

The resulting finite force elements can be calculated by subtracting them with the downforce distribution based on the spanwise mass of the whole wing group:

$$Q_r = Q_{aero} - Q_{fuel} - Q_{structure} - Q_{engine} = 69173.3N$$

The wing can be substituted as a bending beam which is attached to the fuselage frame lugs via bolts with an inner attachment point and an outer attachment point. The wingbox is joined with the different frames of the fuselage. Using in total four pin lugs for one side of the wing the following loads can be obtained:

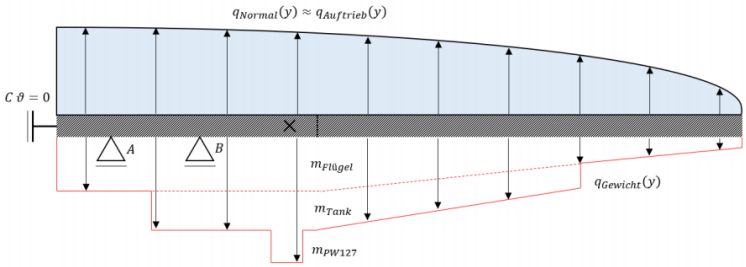

Figure 4-13: Bending Beam Model

$$Q_{inner} \approx 120\ kN\ Q_{outer} \approx 150\ kN$$

The airframe is designed around one main idea: use the latest thermoplastic composites wherever they will make the biggest difference and use smart metal only where it is really needed. The pressurized fuselage is made of a carbon-fiber/PEKK semi-monocoque. The barrel sections are put together using a process called automated fiber placement. They are then fused together with induction-welded joints that don't need fasteners. This makes them as strong as aluminum but much lighter and easier to assemble.

A large rear cargo door is cut straight out of the same laminate. The skins are formed using a press, the inner spars are welded on in one step, and the door is hung on hinges made of printed titanium. These hinges can handle the most weight without adding extra bulk, and they keep the outline of the door smooth and light. A ring made of metal that has been joined using a special process around the opening of the door spreads the pressure of the door back into the composite shell without causing any hot spots.

The tail consists of two thermoplastic half-shells that form torsion-box stabilizers. These are welded along the perimeter to prevent leaks and are joined by titanium lugs that are manufactured using an additive process. These lugs connect the control surface hinges.

The landing gear is made of metal, for the high strength and stiffness. A steel main strut is used to support the STOL work. All other links are made of titanium.

All four solutions, thermoplastic primary structure, welded composite door, hybrid composite tail, and hybrid-metal landing gear, are already flying in demonstrators today. They will be fully certified and ready for production well before the aircraft's planned 2035 entry into service.

4.3 Empennage

For the selection of an appropriate tail geometry the following decision matrix is used:

Table 4-1 Decision matrix for empennage design

Factors	W	T-Tail	Conv.	Cruciform	H-Tail	V-Tail	Inv V-Tail
Drag	3	+	0 (1,04)	-- (1,06)	-- (1,06)	+ (1,03)	+ (1,03)
Ground Access	3	0	0	0	-	0	--
Stability	5	++	0	+	+	-	-
Control	4	0	0	0	-	--	--
Weight	3	--	0	-	--	+	+
Nom. AOA	3	++	0	+	0	0	+
High AOA	5	--	0	0	0	0	+
Sum		3	0	-1	-14	-7	-5

Figure 4-14: Aircraft C.G. & AC Location

The aircraft must provide static stability on the one side and should be trimmable on the other side in the whole span of its expected operational envelope. This can be done based on the momentum equilibrium around the approximated C.G. position of the aircraft (simplified version given in [6]). With the use of the tail volume method based on statistical data and the following equation the allowable C.G. shift, surface area of the horizontal and vertical tail can be calculated:

$$M_{CG} = M_W + L_W * x_{CG-AC} - L_H * (l_H - x_{CG-AC}) + M_H - T * z_E$$

Considering the landing configuration with highest thrust achievable (Go-Around) with an additional static margin of 0.1 based on statistics [6], the aircraft C.G. travels between 5% and 41% MAC. Leading to an average position of $x_{CG,A/C} = 10.26m$ and a surface area of the horizontal area of $S_{HT} = 15.33m^2$.

The vertical tail sizing is based on the one engine inoperative case at highest thrust with the minimum control speed, which is also defined by the certification specification. This leads to a vertical tail area of $S_{VT} = 10.48m^2$ with the dorsal fin.

The incidence angles of the horizontal tail and the wing group adjusted individually to achieve a zero-moment coefficient at the design lift coefficient of 0.4. Moreover, to validate static stability, a dC_m/dC_L gradient of nearly the static margin at the most aft position can be obtained.

4.4 Landing Gear

This section describes the sizing process carried out for the design of the landing gear. The process enclosed is highly relied on the guidelines and empirical data shared by Raymer. [6] Before the preliminary sizing it is important to consider the available configurations for landing gear. A thorough comparison was made which can be represented by the following decision matrix. The weighting factors were assigned according to the extent to which each criterion contributes to meeting the TLAR.

A fuselage-mounted tricycle landing-gear configuration was selected because the aircraft employs a high-wing layout; any wing-mounted gear would impose an unnecessary weight penalty. The tricycle arrangement also keeps the aircraft nearly horizontal on the ground, ensuring unobstructed cockpit visibility during taxi, takeoff, and landing being an essential feature for AETHER, which must operate on runways that may be littered with debris or other obstacles in emergency situations.
This configuration improves passenger comfort, a high priority because AETHER will transport injured patients on stretchers and must provide sufficient space for medical personnel to work effectively and ground levelled. It also permits stable two-point landings at high angles of attack, reducing approach speeds and enabling operation from short runways.

Moreover, the tricycle gear shows no tendency to bounce or overturn and offers excellent directional stability, protecting fragile medical equipment and vulnerable passengers. Although the design is somewhat more complex, costly, and voluminous than simpler alternatives, these disadvantages are outweighed by its operational advantages.

Given that AETHER cruises above Mach 0.3, a retractable landing-gear system was adopted to minimize drag and maximize performance. Because the fuselage section is too compact to house the main gear entirely without encroaching on cabin volume, a fuselage-podded junction was implemented, preserving valuable cabin space for passenger comfort. In addition, oleo-strut shock absorbers were chosen for their proven reliability in the aerospace industry, offering lower cost, simpler design, and reduced weight and volume compared to trailing-link alternatives.

The landing-gear sizing proceeded iteratively, beginning with initial station assumptions based on comparable aircraft layouts and refining each component's mass and balance until the full-aircraft center of mass converged on the current design iteration. A detailed comparison of center-of-mass excursions across the three mission profiles during static (boarding/un-boarding) and dynamic (take-off/landing) phases identified the most forward and aft CG positions. For the dynamic cases, nose-gear load limits of 8-15 % at the forward-CG extreme and 12.80% at the aft-CG extreme defined the longitudinal placement of the main and nose gear, as illustrated in figures 4-15 through 4-16 and as recommended by statistical 8-15% limit load distribution for the nose gear. Static tail-down, overturn, and tail-strike angle criteria were then applied to verify ground-handling stability. [6]

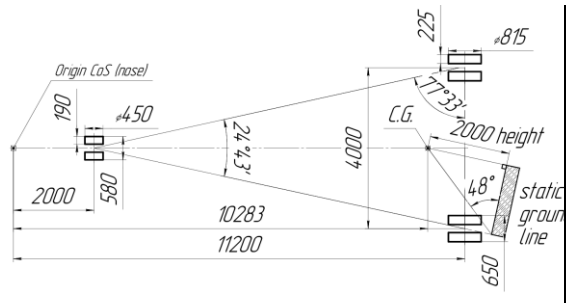

Figure 4-15: Landing gear layout up-view

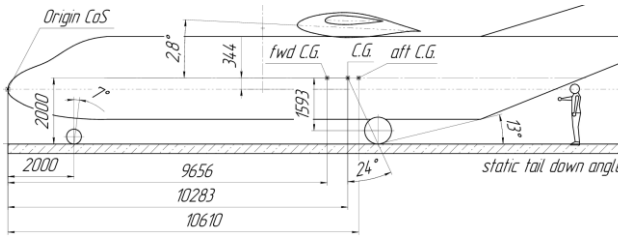

Figure 4-16: Landing gear layout: side-view

Tire dimensions were initially estimated using a statistical tire-sizing method [6]:

$$Tire\ diameter\ or\ width\ [in.] = A * {m_w}^B;$$

Where A and B are statistical constants and m_W correspond to the total mass carried by one main or nose tire.

$$m_w^{nose} = \frac{m * M_f}{b * n_{nose}} \; or \; m_w^{main} = \frac{m * N_a}{b * n_{main}}$$

m – corresponds to the total mass of the aircraft, n_{nose} , n_{main} – the number of tires per nose or main landing gear respectively, b – is the wheelbase, M_f – is the distance between the most aft center of gravity and the main landing gear and N_a – is the distance between the most aft center of gravity and the nose landing gear.

The braking-friction-limited force component was incorporated to account for landing deceleration and runway-length requirements. [14]

$$F_b < F_{total}$$

$$\frac{m * V_L^2}{2 * s} < F_{braking} + F_{aerodrag} = \mu * m_w + 0.5 * \rho * V_L^2 * C_{D_L} * A_{wing}$$

It was found that the required brake force was fulfilled for each mission's runway length (s), coefficient of friction (μ) and atmospheric conditions without using reverse thrusters even though they are available. The total landing drag coefficient C_{D_L} was calculated for every scenario using vortex-lattice simulations with VSP Aero and validation with handbook methods.

The first mission scenario with $\mu = 0.05$ and $s = 756m$ at an altitude of 2850 m above MSL and ISA +20° proved most demanding and set the design tire load. Final tire selection was made by comparing these loads to commercially available catalog sizes, choosing the option most closely matched to similar aircraft. Tire numbers M13201 Michelin Air X and 026-545-0 Michelin Air are selected for the main and nose landing gear respectively.

4.5 Propulsion System

4.5.1 Evaluation of Design Space

The trade study, shown in, compares different combinations of energy sources and propulsor systems. The trade study assumes there is sufficient energy onboard the aircraft to meet the aircraft's range requirements, which is balanced by the penalties incurred in the weight criteria. Three different hybrid propulsion concepts were analyzed. The battery hybrid and fuel cells hybrid concepts utilize a system architecture where the electric energy source and fuel burning gas turbine are both connected to an electrical generator which distributes its energy to electric motors, thus enabling distributed propulsion. For the electric hybrid, the batteries would be used during take-off and climb and then charged by the turbine engine during cruise. The fuel cells, which actively generate power during flight and therefore are more effectively used to assist the turbine engine during the cruise phase. Another hybrid propulsion concept considered is a fuel cell battery hybrid, where both fuel cells and batteries are connected in series to electric motors that drive the propulsors. This system architecture enables distributed propulsion and allows the batteries to be charged by the fuel cells during cruise flight after being used for take-off and climb segments, thus effectively balancing the high energy density and low power density of fuel cells with the opposite characteristic of batteries. The safety aviation fuel (SAF) and Jet A-1 fuel propulsion concept utilize the conventional system architecture, with gas turbine engines that burn fuel to power the propulsors.

Table 4-2 Decision Matrix for Propulsion System

Criteria	wt.	Energy Source + Powerplant					
		Jet A-1 + GT	SAF + GT	SAF/ Battery + E-motor/ GT	SAF/ FC + E-motor/ GT	FC/Battery + E-motor	Battery + E-motor
Op. Envelope	10	++	++	+	+	-	--
Weight	10	++	++	0	+	-	--
Emissions	8	--	0	+	+	++	++
Cost	8	++	++	+	-	--	0
Noise	6	--	--	0	0	++	++
Reliability	6	++	++	+	0	--	-
Total Score		40	56	32	20	-20	-18

For MEDEVAC operations the primary goal is to save lives, with high speed, long range, rapid response critical for reaching and delivering care to patients within life-saving timeframes. Increasing efficiency directly relates to minimizing fuel consumption, subsequently maximizing payload and range, thus leading to increase the operational flexibility. Maximizing performance is crucial for reaching the emergency destination as fast as possible, therefore, meeting the TLAR's (operating envelope) in the most efficient (weight) method possible was considered the key objective of the propulsion system (weighting = 10). With the aviation sector pushing to meet its 2050 climate targets and the well-known importance of economic viability in commercial success, sustainability (emissions) and feasibility (cost) were deemed as second most critical considerations in the propulsion system choice (weighting = 8). For MEDEVAC aircraft operating in both remote and challenging environments, the noise and reliability of the propulsion system are also important factors, hence they were included in the criteria (weighting = 6).

The results of the trade study show that a conventional gas turbine engine powered by SAF was the best performing propulsion system, with both the battery and fuel cell hybrid systems scoring lower. This is primarily due to the low energy density of batteries relative to SAF which directly relates to reduced efficiency, even with an ambitious prediction of the 500 Wh/kg for energy density of solid-state batteries assumed possible for entry into service by 2035 considered [15]. The batteries also have a relatively narrow range of temperatures in which they can operate efficiently [15], limiting their performance in extreme conditions, which is an important requirement for a MEDEVAC aircraft and thus reduces its reliability and performance scores. The overall increase in system complexity and cost to implement an appropriate thermal management system for such extreme conditions also impinges cost and reliability scores. Fuel cells also have similar issues, with a reduced operating conditions envelope due to low air densities at higher altitudes restricting their efficiency [16]. The additional infrastructure required for storage and thermal management of a hydrogen and fuel cell system is a major penalty for cost, reliability, and efficiency. The slow start-up and discharge rates of fuel cells also significantly reduce their performance during take-off and climb, which is vital for MEDEVAC operations which require fast response times [17].

100% SAF fuel can be implemented with no additional infrastructure or modifications to the PW127 model engines, with it already successfully trialed on the ATR72 [18], thus proving it reliability as a power source. Currently Alcohol-to-Jet Synthetic Paraffinic Kerosene (ATJ-SPK) is certified to use in gas turbine engines, with an energy density slightly higher than the Jet A-1 fuel (44.0 MJ/kg vs 42.9 MJ/kg [19]) resulting in increased efficiency. SAF also provides higher air quality than Jet A-1 fuel with less particulate matter emissions and a emissions reductions factor of approximately 80% [20]

Overall, a convention turboprop engine powered by SAF was deemed to be the optimal propulsion system balancing the performance requirements, with efficiency, sustainability, cost, noise and reliability.

4.5.2 Engine Selection

An already existing engine was selected from the current market so the aircraft could be designed around known specifications and available performance data. Using proven engine technology with an existing supporting network makes maintenance easier, reduces the technical risks and thus increases the reliability of the engine which are all key factors for a MEDEVAC aircraft operating in remote areas. A trade study was performed for both two and four engine configurations, using engines from different manufacturers, with different powers, sizes and weights. The ratio of maximum continuous power to engine dry weight was the main selection criteria which drove the decision to select a twin turboprop set up using the Pratt & Whitney 127G. The engine is currently fitted to the CC-295 Kingfisher which is used by the Royal Canadian Air Force for search and rescue operations, thus demonstrating it capability to operate in rough remote airstrips at freezing temperatures which is ideal for a MEDEVAC aircraft [21]. PW127G's high continuous power output (2178 kW) combined with its low shaft speed (1212 RPM), enables the aircraft to cruise at higher speeds before running into issues with propeller wave drag [22]. With ATR and Pratt & Whitney announcing in June 2025 its collaboration on propulsion technology to advance the next generation regional turboprops [23], it is assumed a more efficient, durable and reliable engine model will be used instead of the model (PW127G) used for this preliminary design study.

4.5.3 Engine Position

The engine is positioned underneath the wing, at 3.64 m from the fuselage longitudinal axis, maintaining a propeller tip clearance of 0.69 m from the fuselage, the same as the reference aircraft, ATR42. The engine is positioned 0.2 m below and 1.2 m in front of the wing leading edge, ensuring the engine does not interfere structurally with the main wing box of the wing whilst also positioning the propeller slipstream in an optimal position to utilize the blown wing effect [24]. The underwing positioned provides the propeller with

free-stream undisturbed airflow, whilst also providing bending relief to the wing which reduces its required structural weight. The high wing design provides the propeller with a 1.5 m ground clearance thus reducing the risk of FOD, a key consideration when landing on remote airstrips with unpaved runways.

4.5.4 Propeller Design

Table 4-3: Specifications of propeller design

Diameter	Taper	Sweep	Blades	Material	Control type
3.4 m	0.27	5°	7	Composite, nickel alloy leading edge	Hydromechanically controlled - variable pitch, reversible, fully feathering

The basic properties of the propeller the modelled blade design are shown above in Table 4-3 and **Error! Reference source not found.** respectively. The propeller was designed with reference to the 3,93 m, 6 bladed Hamilton Standard 568F propeller, used by the ATR42 which cruises at the same height and speed with the same engine class (PW127) . The design also takes inspiration from the MT-47 propeller, which is fitted to the Pilatus 12, an aircraft commonly used for MEDEVAC operations [25]. The MT-47 uses a 7-blade composite design with a nickel alloy leading edges for superior erosion protection and compared to the previous 4-blade model it reduces the interior cabin noise by up to 6 to 8 dB (A) and the ground roll distance by 20% [26]. A major advantage of a 7-blade design is the higher solidity ratio which reduces aerodynamic blade loading. This allows the propeller to utilize more of the engine's power without risking aerodynamic stall during take-off. The resultant higher static thrust is a key requirement for STOL aircraft and thus was a major factor in the design. The higher blade count also increases the blade passage frequency (BPF). This shift towards higher tonal frequencies is shown to reduce the perceived loudness of the propeller [27], which is another key factor in the design. The ground roll and noise data improvement displayed by the MT-47 provide validation for the choice of a 7 bladed design.

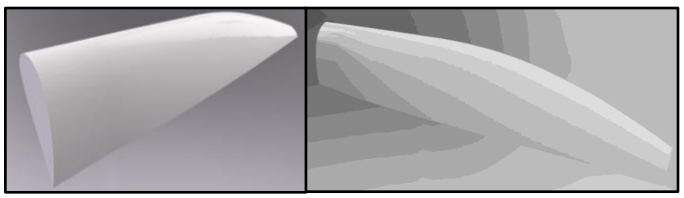

Figure 4-17: Propeller design from PropCODE [29]

A 3.4 m blade diameter was calculated based on analysis of the Mach tip speed in the aircrafts cruise condition, over the range of air conditions dictated by the TLAR's, ensuring the propeller doesn't suffer from wave drag. The propeller blades have swept and tapered tip design emulating a scimitar blade. The sweep reduces the effective Mach number at the blade tip, limiting it to 0.85 to prevent wave drag [28]. When cruising at maximum speed in ISA-35 conditions the propeller RPM must be reduced by 7.5% to prevent wave drag, reducing the flight speed to 133 m/s (2.5% reduction). According to the situation, the pilots can further reduce the propeller RPM if they decide to prioritize cabin noise over aircraft speed.

The design of the chord, twist and airfoil distribution was optimized using PropCODE, a MATLAB tool that designs and simulates propellers [29]. The design part of the software utilizes blade element theory to generate a blade profile with minimum induced losses (MIL) given a set of boundary conditions (design point). Different design points were formulated according to the various flight phases and the mission conditions which dictate the air condition and engine power. These design points were subsequently inputted into the MIL designer to generate the MIL chord and twist distributions and resultant lift-to-drag (L/D) distribution as shown in **Error! Reference source not found.**0.

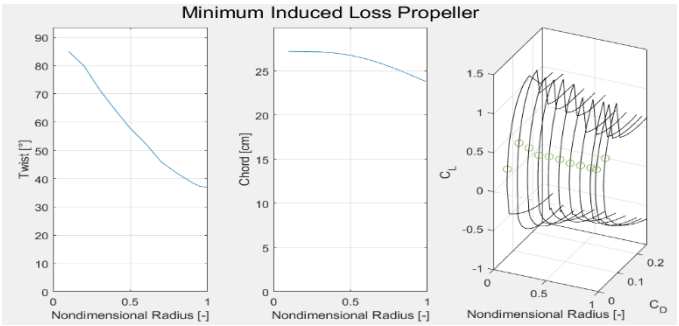

0.1000	NACA3625
0.2000	NACA3622
0.3000	NACA3519
0.4000	NACA3417
0.5000	NACA3415
0.6000	NACA3415
0.7000	NACA3412
0.8000	NACA3412
0.9000	NACA3412
0.9500	NACA3412

Figure 4-18: Propeller data from PropCODE

The root chord, taper ratio and airfoil distribution define the geometric boundary conditions. A sensitivity study of these geometric parameters was performed based on the power output and L/D results from the MIL designer. The power output was used to ensure the blade has a large enough chord to utilize the full engine power, whereas the L/D was used to find the optimal NACA airfoil profiles along the blade span. Structural factors were also considered when designing the airfoil distribution, with thicker airfoils placed at the blade root due to the higher bending moment and torsional loading.

The twist and chord distributions at each of the design points were averaged based on the mission time spent in each flight phase, thus producing a time-weighted average distribution for each mission. The different mission conditions were then probability averaged, assuming the likelihood of flying in each condition as 80% in ISA+5, 10% each for ISA -35 and ISA+20, thus providing a singular set of results for twist and chord distribution, shown in **Error! Reference source not found.**. The results from PropCODE were then exported as coordinate point to CATIA, a 3D CAD software, where the blade was modelled, as displayed in

4.6 Aircraft Systems

The aircraft will apply a More Electric Aircraft (MEA) systems architecture which utilizes purely electric power to drive the non-propulsive aircraft systems, without using bleed-air from the engines. Streamlining the power source to all aircraft systems increases the energy efficiency of the aircraft, resulting in an estimated 3% increase in fuel efficiency [30], whilst also greatly reducing the system complexity. This is achieved by removing the hydraulic pump and compressor bleed air system from the engine, thereby reducing power extraction losses, as well as removing the hydraulic pipes and gas ducts which they used to distribute power. The aircraft's systems will be powered by variable frequency generators directly connected to the accessory gearbox of the engines, as shown in **Error! Reference source not found.**1.

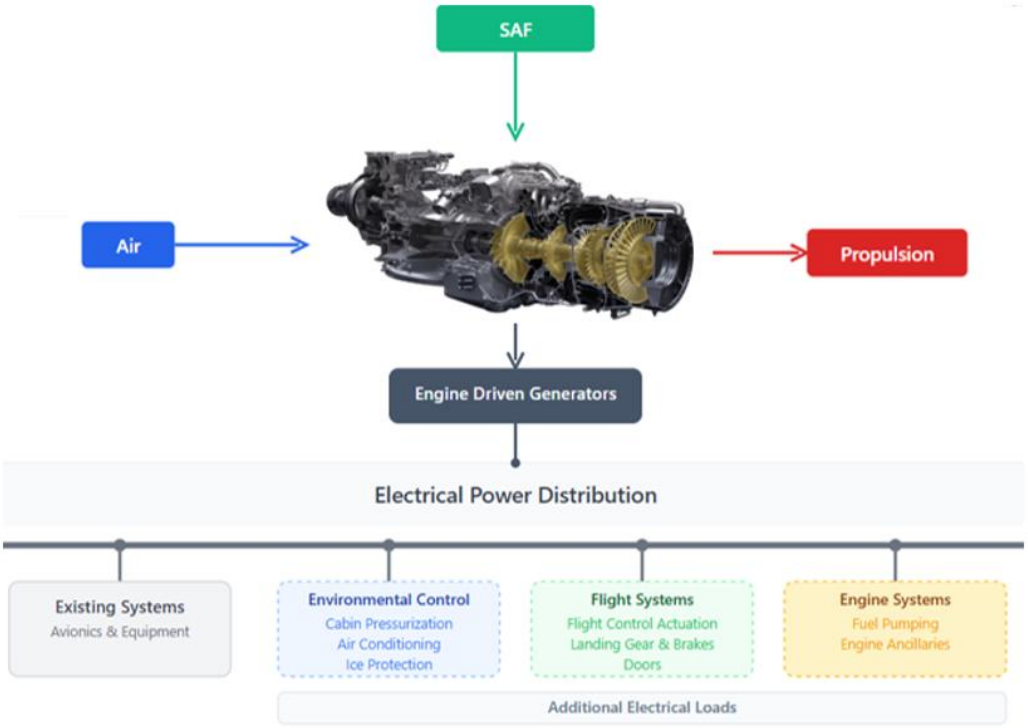

Figure 4-19: MEA system architecture integration with turboprop aircraft

The estimated power required for all non-propulsive aircraft systems during cruise, the most energy intensive flight phase, was determined as 80 kW by extrapolating the results of [31] and adding a 10% margin for medical equipment power load. Most flight systems utilize electro-mechanical actuators, however, the systems with higher loads, identified in Table 4-4Table 4-4, require higher power density electrohydraulic actuators.

Table 4-4: Aircraft flight systems with their related primary components

System	Primary Components
Ailerons, rudder, elevators, slats	Electro-mechanical actuator
Flaps	Electro-hydraulic actuator
Brakes	Electro-mechanical brakes
Nosewheel steering	Electro-mechanical actuator
Landing gear	Electro-hydraulic actuator
Cargo door	Electro-hydraulic actuator
Fuel Pumping system	Electric fuel pumps
Environmental Control System (ECS)	Electric compressor, electric air conditioning pack, electronic control unit
Ice protection system (IPS)	Wing: Electro-Mechanical Expulsion De-icing System (EMEDS) Propeller: Electrothermal de-icing boots

The selection of the ice protection system was based on balancing the effectiveness of ice protection with its power demands whilst also considering the performance level required. Whilst electro-thermal anti-icing system is the most effective way of preventing ice-formation on the leading edge of surface, considering MEDEVAC aircraft have no set route, thus the conditions they fly in vary from mission to mission, the aircraft will not fly in extreme icy conditions regularly enough to justify the high-power requirements of such a system. Instead, low power mechanical de-icing systems will be used, both for the wing leading edge. Electro-Mechanical Expulsion De-icing System (EMEDS) will be implemented to protect the leading edge of the wing against ice build-up, using only 300 W/m span [32]. It utilizes millisecond high current electrical impulses to vibrate an erosion shield layer at high frequencies to de-bond accumulated ice [32]. Electro-thermal heated wire de-icing boots are used for the propeller, with electric pulse vibration technology not anticipated to be ready by 2035 at the reliability and durability levels required for a MEDEVAC aircraft.
The largest system transition between a conventional and a MEA aircraft is the environmental control system (ECS), which no longer is supplied by engine bleed-air, and thus requires a separate electric compressor. The ECS system is located on the forward belly of the fuselage, with the air inlets strategically placed to reduce the internal air ducting length and complexity. The ECS will consist of two compressors, each with its own air conditioning pack to provide redundancy. The compressors are sized for 60% of the air flow demand, optimizing power management through load sharing and reduction of peak power relative to one big unit. An electronic control unit manages the ECS system, using temperature and pressure sensors together with a valve network to regulate the flow rate and condition of air entering and exiting the cabin.

The electric compressor air inlets have been positioned at the front and top of landing gear fairing, away from wing and propeller slipstream to avoid any turbulent interference. The air inlets will be symmetrical to provide redundancy for blockages. The internal airduct system connects both inlets to both compressors for redundancy, with valves used to direct the flow as required. They are placed in front of the main landing and off the propeller axis to reduce the risk of foreign object damage (FOD). To further reduce the risk of FOD the compressor air inlets will sit recessed inside curved front section of the landing gear fairing, it will also utilize a low drag mesh with 60% open area. For the heat exchanger in the air condition pack a ram air inlet will be used, positioned directly below the ECS on the front belly of the fuselage.

Due to the positions inherent exposure to FOD an inertial separator will be integrated, with a mesh screen also used to block out debris. An electric fan will be placed inside the ram air inlet draw in air during ground operations. The air outlet for ventilation of cabin air will be placed adjacent to the ram air inlet with the same mesh screen used to reduce risk of FOD. The ECS will pressurize the cabin to 6000 ft when cruising at 25000 ft, with the rigid composite fuselage structure enabling a higher-pressure differential than traditional aluminum airframe [33]. For patients requiring sea level pressure due to a specific medical condition the aircraft can reduce its altitude to 15000 ft, where the ECS, by maintaining the same pressure differential, provides the cabin with sea-level pressure.
The aircraft will have an auxiliary power unit (APU) located in the tail cone. It will provide power for the ECS and medical equipment before the engine starts or while waiting on the ground, which is critical for remote locations where ground power may not be available. Using an APU also avoids running the main engines whilst on the ground, saving fuel and engines cycles. It will also be used to start-up the main engines by providing power to the engine starter generators. The ability to self-start provides operational flexibility and enables a faster start-up time which is critical in MEDEVAC missions. The APU will be sized so its capable of generating 80 kW, to enable full in-flight redundancy for all aircraft non-propulsive systems. A main battery will be used for the APU start-up and as a power source of short period peak loads, with a

smaller emergency battery required for redundancy, like the battery configuration of the of ATR 42 [34]. This allows the battery to perform small tasks, like avionics boot up, without requiring the APU to run, with the engine generators recharging the battery during flight.

5. Technical Report

5.1 Three-side view

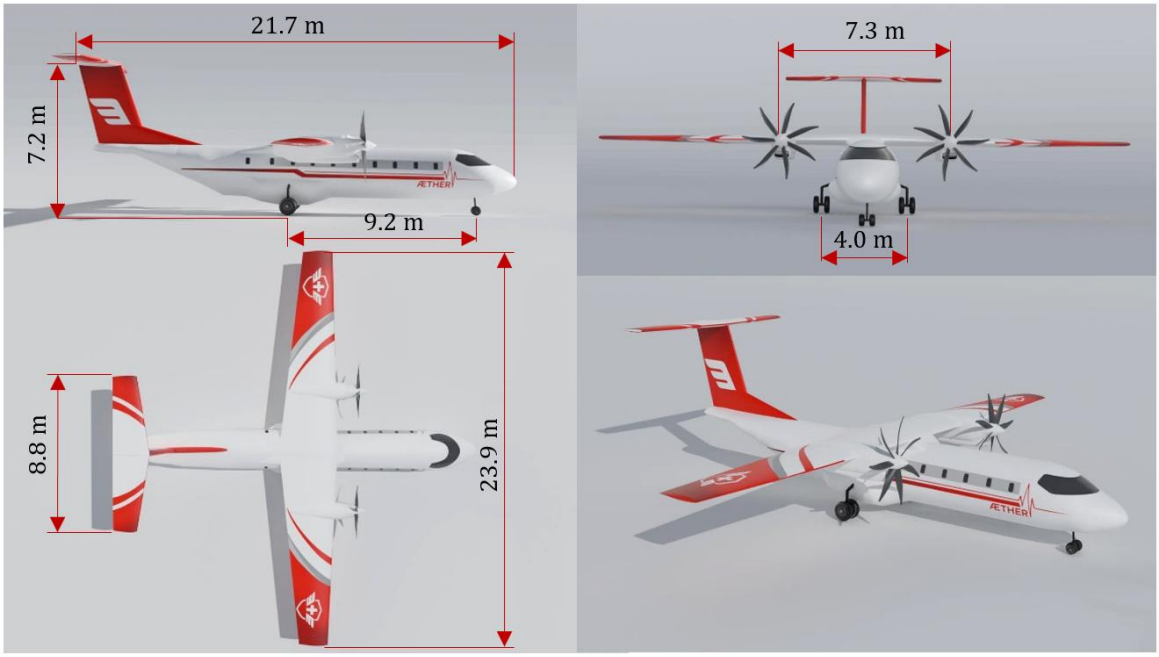

Figure 5-1: AETHER in three-side view

5.2 Key technologies

The objective of designing a pressurized turboprop MEDEVAC aircraft for entry-into-service (EIS) in 2035 is ambitious but attainable. The program should prioritize technologies that can be advanced to Technology Readiness Level (TRL) 8-9 within the next decade and direct less mature concepts to parallel Research and Technology (R&T) tracks.

Technologies that can credibly reach operational maturity by 2035:

- **Propeller-blown, double-slotted Fowler flap + full-span slat high-lift system (TRL 9):**
  Recent wind-tunnel and CFD campaigns demonstrate that a conventional two-element flap immersed in the propeller slipstream can enhance $C_{L,max}$ by 40% while maintaining pitching-moment penalties at a manageable level [48].
- **"More-Electric" secondary systems (TRL 8-9):**
  The transition of bleed-less electric environmental control systems, electrically driven pumps, and electro-mechanical actuators from bench-top testing to flight operations has been successfully implemented on aircraft models such as the Airbus A320neo. A study of the optimization of electric ECS architectures for civil aircraft reveals that there are no significant impediments for the 500-kW power class that are relevant to a regional MEDEVAC airframe [49].
- **100 % Sustainable Aviation Fuel (SAF)-ready 2 MW turboprop engines (TRL 9):**
  ATR and Pratt & Whitney Canada have already completed flight tests with neat SAF in PW127-series engines and are working toward full fleet certification before 2030 (ATR source). The integration of such engines is primarily a process involving seals, fuel-temperature management, and administrative tasks [50].
- **Rapid-reconfigurable, pressurized MEDEVAC cabin (TRL 8-9):**

Patent-protected quick-change rails and drop-pin seat-track adapters allow a swap from passenger to stretcher ICU layout in under 30 minutes without special tooling, as already offered in commercial kits by Spectrum Aeromed and others (Google Patente). Certification effort focuses on crash-load paths, oxygen distribution and EMI compatibility of life-support equipment [50].

- **Robust, multi-terrain trailing-link landing gear with low-pressure tires (TRL 9):**
  The utilization of patent-protected quick-change rails and drop-pin seat-track adapters facilitates a rapid conversion from a passenger to a stretcher ICU layout, a process that can be executed in less than 30 minutes without the necessity of specialized tooling. This capability has been previously offered in commercial kits by Spectrum, Aeromed, and other manufacturers, as evidenced by patent searches on Google. The certification process places particular emphasis on crash-load paths, oxygen distribution, and electromagnetic interference (EMI) compatibility of life-support equipment.

Attractive concepts that will still be ≤ TRL 5 by 2035:

- **>1 MW hybrid-electric distributed propulsion:**
  While it offers significant STOL and noise advantages, NASA's roadmap places TRL 6 only in the late-2030s. The challenges of thermal management and certification for large batteries remain unresolved.
- **Liquid-hydrogen PEM fuel-cell powertrains:**
  Companies such as ZeroAvia are conducting ground and flight demonstrations, yet full-scale, crash-worthy cryogenic tanks and 2 MW stacks are not expected to attain transport category certification before 2040.
- **Morphing, smart-material high-lift surfaces:**
  Despite the assurance of seamless lift devices, challenges persist regarding actuator fatigue life and fail-safe criteria, thereby constraining their advancement to approximately TRL 3–4 through the 2030s.

5.3 Weight & Drag of Subsystems

The aircraft's weight was estimated using Kundu's [35] method and cross-validated the results with multiple Class I and II techniques—namely Raymer [6], Loftin [36], Torenbeek [37], the USAF standard procedure [13], and Gudmundsson's approach [38]. The final weight figures were then adjusted according to [6] reflecting the reductions enabled by the advanced technologies available in 2035, the MEA tendency of integrated technologies into this design and the discrepancies of using methods highly based on old statistical data.

Table 5-1 - Mass breakdown of aircraft's main components

Component	Mass [kg]	Mass [MTOM%]	Longitudinal position [m]
Wing and HLD	1711.26	0.1222	10.010
Vertical Tail	90.28	0.0064	18.200
Horizontal Tail	421.45	0.0301	20.670
Fuselage	2742.94	0.1959	9.933
Main Landing Gear	478.80	0.0342	11.200
Nose Landing Gear	53.20	0.0038	2.000
Nacelle	31.25	0.0022	9.345
Installed Engine	1346.24	0.0962	9.345
Systems and Flight controls	2289.00	0.1635	9.933
Σm – MEM	9164.42	0.6546	10.48
Pilots and Pilot seats	194	0.0139	2.170
Σm – OEM	9358.42	0.6685	10.283
Payload mass	0 - 2500	0 – 17.86	8.650
Σm – MZFW	11 858.42	0.8470	10.283
Fuel mass	0 - 3880	0 – 0.2771	10.260
MTOM	14 000	1	10.229

Given AETHER is a highly modular aircraft that adapts to different flight missions, it was decided to consider equipment that would normally be counted as OEM as payload to portray more accurately the mass that is variable between missions and what is fixed to operate the aircraft. Such mentions include but are not limited to passenger stretchers and seats, installed cabinets and galley.

Drag

For a subsonic aircraft the drag of it subsystems can be broken down into two components zero-lift drag and induced drag. The induced drag of the aircrafts subsystems was calculated by simulating the aircraft on OpenVSP. The simluations were performed over a range of angles of attack's (AoA) in the conditions imposed by the mission scenarios, with lift and drag polars extracted from the results. The zero-lift drag, C_{D0}, was calculated using the drag build up method, using the following equation:

$$C_{D0} = \sum_{c}^{n} C_{f,c} \cdot FF_c \cdot Q_c \frac{S_{wet,c}}{S_{ref}}$$

Where C_f is the skin friction coefficient, FF is the form factor, Q is the interference factors and $\frac{S_{wet}}{S_{ref}}$ relates the drag coefficient of the component, *c*, to wing reference area.

All *n* components (denoted, *c*) are considered; however, certain effects are difficult to calculate using these methods, therefore, their drag coefficients are added separately. For take-off and landing the drag of the flaps and landing gear are also added, with equations provided by Loftin, 1980 [39]. Table x shows the components, and their individual zero-lift drag, calculated using the drag build up method for scenario 1 in the clean configuration.

Table 5-2 Zero lift drag breakdown

$Total_{clean}$	Fuse-lage	Wing	Nacelle	Propeller	H-tail	V-Tail	F-up-sweep	Misc.
0.026	0.00544	0.00794	0.00189	0.00091	0.00226	0.0013	0.00411	0.00211

5.4 Mission Parameters & Performance

This section outlines the critical mission parameters that define AETHER's operational capabilities and energy demands, as derived from the top-level requirements. Key performance metrics such as climb and descent rates, cruise altitude and speed, and primary aerodynamic and propulsion characteristics (including lift-to-drag ratio and specific energy consumption) are presented through detailed table 5-3 and figures 5-2 through 5.6. These data form the analytical basis for validating mission performance, conducting payload–range trade studies, and sizing the propulsion and energy systems.

The payload–range diagram in figure 5-4 was derived using statistical fuel fraction estimates for each mission segment, based on Roskam I [7]. These fuel fractions were applied relative to the Maximum Takeoff Mass (MTOM) to determine overall fuel consumption across various mission profiles. The Breguet range equation was employed to compute the fuel burn and achievable range during cruise, loiter, and diversion phases. These calculations utilized the cruise speed defined in the matching diagram, as well as revised lift-to-drag ratios for cruise and loiter, obtained from OpenVSP Aero's Vortex Lattice Method and validated against classic bluild up drag estimation techniques from literature. The engine's specific fuel consumption (SFC) was taken from manufacturer data for the selected powerplant. Additionally, the loiter time was prescribed according to EASA emergency diversion regulations, ensuring regulatory compliance for medical evacuation missions.

By quantitatively linking aerodynamic efficiency with propulsion performance, the analysis highlights fundamental trade-offs among endurance, speed, and cruise altitude. The comparative visualization of different mission scenarios facilitates informed design choices and supports the development of robust flight-control and energy-management strategies. The following materials are presented to support this analysis.

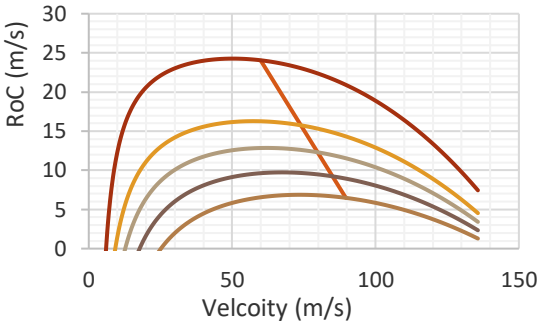

Figure 5-2 - Climb performance Mission 1 outbound

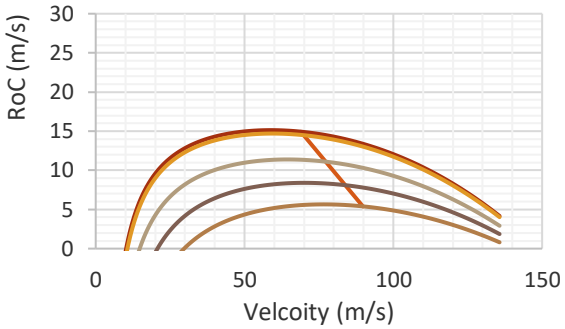

Figure 5-3 - Climb performance Mission 1 return

Table 5-3- Mission profiles and fight parameters

Scenario	1		2		3	
Flight mission	Outbound	Return	Outbound	Return	Out-bound	Return
Required total mission time [h.]	1.5		3.5		9	
Delivered total mission time [h.]	0.78		2.12		5.60	
Turnaround time [min.]	0	10	0	10	0	25
Range radius [km]	153		400		1 250	
Minimal TOFL and LFL [m]	-	756	-	1250	-	1000
Ground altitude MSL [m]	0.00	2850	0.00	0.00	0.00	150.00
Atmospheric condition	ISA +20		ISA -35		ISA +5	
Passengers	4	7	4	19	2	3
Specialized Cargo [kg]	0.00	0.00	500.00	0.00	0.00	0.00
Total Payload [kg]	582.00	982.00	1 664	2 364	405.00	485.00
Fuel required [kg]	2704	1352	2976	1488	3880	1940
TOM [kg]	12 645	11 693	13 998	13 210	13 643	11 783
Max. Rate of climb [m/s]	24.00	14.92	21.07	22.96	21.76	25.17
Max. climb angle [deg.]	23.57	12.51	19.50	23.54	20.43	25.32
Min Climb speed [m/s]	60.01	68.92	63.14	57.50	62.34	58.85
Cruise speed [m/s]	136.00					
Cruising altitude [m]	4572	4572	7620	7620	7620	7620
Rate of Descent [m/s]	7.62					
Descent angle [deg.]	3.54					
Descent speed [m/s]	123.47					
Glide ratio [-]	16.20					
$(L/D)_{cruise}$ [-]	15.20		15.30		15.22	
SFC_{cruise} [1/h]	0.35					
$(L/D)_{loiter}$ [-]	13.16		13.25		13.18	
SFC_{loiter} [1/h]	0.45					
Cruise Power [kW]	1 735.70		2 592.50		1 970.30	

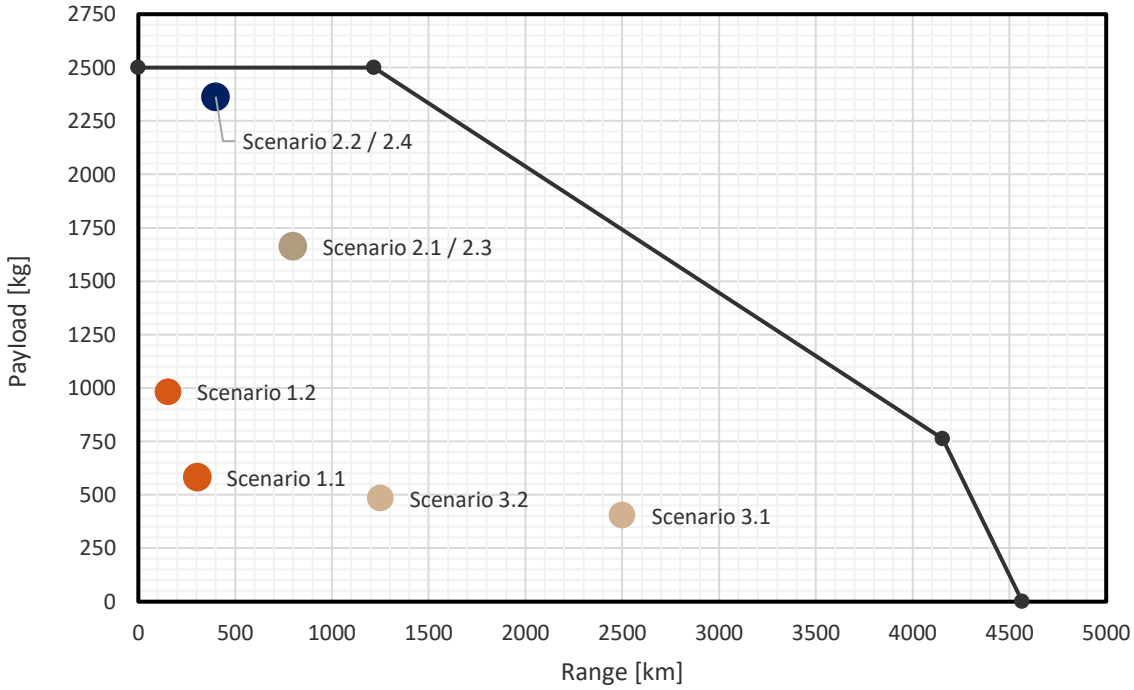

Figure 5-4 - Payload and Range diagram

For clarity and simplicity, the flight envelope in figure 5-5 omits secondary mission segments such as loiter, missed approach, and diversion. However, these phases are fully accounted for in the fuel consumption and range calculations. In compliance with EASA regulations, a 30-minute loiter at holding altitude is included, as well as a diversion segment to an alternate airfield located at 10% of the total mission range. These additions ensure that the performance analysis reflects realistic emergency and contingency scenarios, even if not explicitly depicted in the diagram.

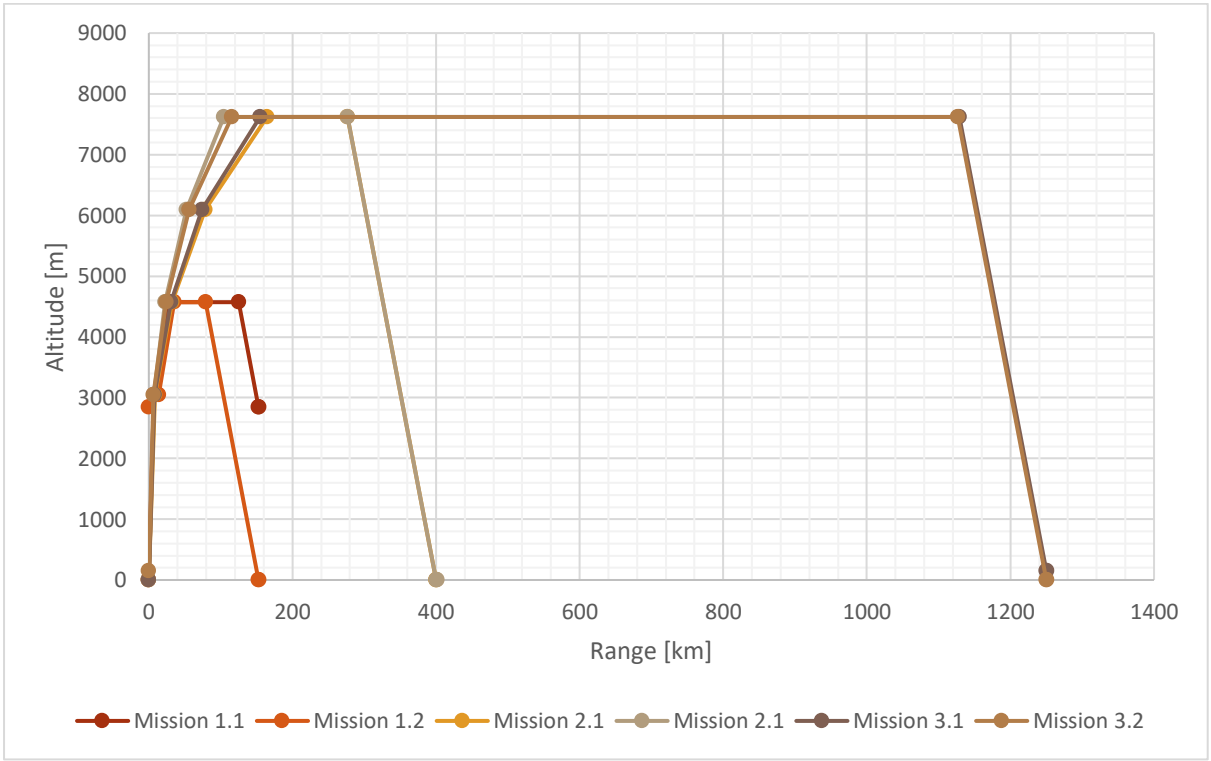

Figure 5-5 - Missions' flight envelopes

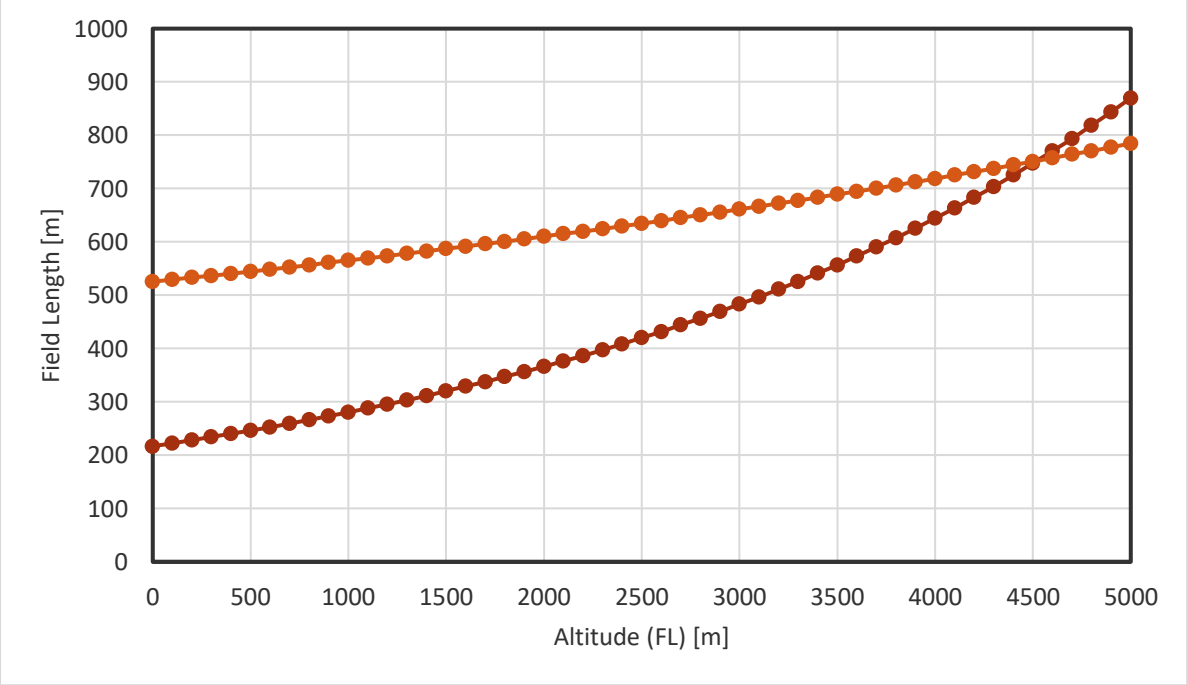

Figure 5-6 - Landing and Takeoff field length performance

6. Conclusion & Recommendations

The AETHER project represents a conceptualization and design of a high-performance regional aircraft tailored for disaster response, medical evacuation, and remote operations. Based on the provided mission scenarios TLAR's were defined and dictated AETHER's design. The cabin space requirements drove the selection of a targeted MTOM of 14,000 kg and the parameters of the aircraft were determined using fundamental aircraft design formulas. AETHER achieves a balanced performance profile suitable for short take-off (STOL) and landing operations as well as long-range missions. Its modular cabin design meets the needs of MedEvac aircraft by optimizing the cabin space for both air-ambulance missions and humanitarian evacuation scenarios. The combination of a cabin railing system and rear loading door makes the design highly modular and enables safe and efficient loading of equipment and highly injured patients, thus reducing response times. AETHER balances sustainability with reliability and efficiency, implementing a More Electric Aircraft systems architecture and using sustainable aviation fuel for its high-power turboprop engines, selected to optimize the efficiency and performance of the aircraft.

In totality AETHER is rooted in sound technical design, abiding by the CS-25 regulatory framework. The STOL and range requirements defined by TLAR's have been met whilst maximizing performance, efficiency and reliability with its twin-turboprop propulsion system. The interior cabin design has been made highly flexible through the use of rail and clip system as well as spacious. The aircraft's balanced performance characteristics in combination with its spacious and modular cabin design make the aircraft suitable for diverse range of MedEvac mission scenarios.

7. References

[1] X. Liang, N. Tian, D. Lopes Da Silva, L. Scarazzato, Z. Karim and J. G. ricard, "Trends in world military expenditure," SIPRI, Solna, Sweden, 2024.

[2] "Statistisches Bundesamt," October 2024. [Online]. Available: https://de.statista.com/statistik/daten/studie/2617/umfrage/anzahl-der-krankenhaeuser-in-deutschland-seit-2000/. [Accessed July 2025].

[3] G. N. Hawkswell, "The Influence of Propeller Position and Size on the Aerodynamics of Blown Wings," University of Cambridge, 2024.

[4] K. H. Schwabe, "Long–Distance Aeromedical Transport of Patients with COVID–19 in Fixed–Wing Air Ambulance Using a Portable Isolation Unit: Opportunities, Limitations and Mitigation Strategies," Dovepress, 2020.

[5] M. Sarlioglu, "More Electric Aircraft – Review, Challenges and Opportunities for Commercial Transport Aircraft," University of Wisconsin-Madison, Madison.

[6] D. P. Raymer, Aircraft Design: A conceptual approach.

[7] J. Roskam, Airplane Design. Vol. 1 : Preliminary Sizing of Airplanes, Lawrence, Kansas: Analysis and Research , 1989.

[8] DIN, "Medical vehicles and their equipment - Air ambulances - Part 2: Operational and technical requirements forair ambulances: EN 13718-2," DIN, Berlin, 2015.

[9] S. International, "https://www.sae.org/standards/content/as33601/," [Online].

[10] D. R. C. Nelson, "Flight Stability and Automatic Control - Second Edition," WCB / McGraw-Hill, 1998.

[11] A. D. &. L. S. J. H. Abbott, "Summary of Airfoil Data," National Advisory Committee for Aeronautics, Washington, 1945.

[12] A. &. Doenhoff, "Theory of Wing Sections - Including a Summary of Airfoil Data," Dover Publications, Inc. , New York, 1959.

[13] Datcom and D. Hoak, "USAF Stability and Control Datcom," Wright-Patterson Air Force Base, Ohio, 1978.

[14] C. Wang and . F. Holzapfel, "Evaluation of aircraft braking performance based on operational flight data," ICAS, Garching, 2018.

[15] D. M. Tavish Pattanayak, "Battery Technology in Aviation: Current State and Future Prospects," *Applied Energy,* vol. 397, 2025.

[16] F. D. G. T. W. S. B. S. B. C. Willich C, "High-Altitude Operation of a Commercial 100 kW PEM Fuel Cell System," *Energies,* vol. 17 (24), 2024.

[17] I. Buchmann, Batteries in a Portable World, Battery University, 2017.

[18] "ATR successfully performs test flights with 100% SAF in one engine," ATR, 2 2 2022. [Online]. Available: https://www.atr-aircraft.com/presspost/atr-successfully-performs-test-flights-with-100-saf-in-one-engine/.

[19] gevo, "Low-Carbon, Bio-Based Sustainable Aviation Fuel," gevo, [Online]. Available: https://gevo.com/product/sustainable-aviation-fuel/.

[20] Air Transport Action Group, "Waypoint 2050," Air Transport Action Group, 2020.

[21] Government of Canada, "CC-295 Kingfisher," [Online]. Available: https://www.canada.ca/en/air-force/services/aircraft/cc-295.html.

[22] EASA, *TYPE-CERTIFICATE DATA SHEET - for PW100 series engines,* EASA, 2023.

[23] ATR, "ATR and RTX's Pratt & Whitney Canada Collaborate on Propulsion Technology to Advance Next-generation Regional Turboprops," ATR, 16 6 2025. [Online]. Available: https://www.atr-aircraft.com/presspost/atr-and-rtxs-pratt-whitney-canada-collaborate-on-propulsion-technology-to-advance-next-generation-regional-turboprops/.

[24] D. Keller, "Aerodynamic Investigation of the High-Lift Performance of a Propeller-Driven Regional Transport Aircraft with Distributed Propulsion," *Journal of Physics,* vol. Conference Series 2526, 2023.

[25] A. Habib, "7 Operators That Fly The Pilatus PC-12 For Air Ambulance Operations," Simple Flying, 17 2 2025. [Online]. Available: https://simpleflying.com/pilatus-pc-12-air-ambulance-operators/.

[26] Finnoff Aviation Products, "FAA OKs the MT Silent 7," Finnoff, 2021. [Online]. Available: https://finnoff.aero/faa-oks-the-silent-7-mt-propeller-on-the-pc-12-series/.

[27] K. Marte, "A Review of Aerodynamic Noise From Propellers, Rofors, and Liff Fans," NASA, 1970.

[28] F. A. DUBS, erodynamik der reinen Unterschallströmung, 1979.

[29] M. Bergmann, "PropCODEPropeller Comprehensive Optimization and Design Environment,".

[30] M. &. Z. P. &. M. C. Haddad, "Sustainable Aviation: The MEA Case.," 2014.

[31] L. S. B. O. Voth V, "Estimating Aircraft Power Requirements: A Study of Electrical Power Demand Across Various Aircraft Models and Flight Phases," *Aerospace,* vol. 11(12), 2024.

[32] Cox and Company, "Low Power Ice Protection Systems," [Online]. Available: https://www.coxandco.com/low_power_ips.html.

[33] M. Huber, "The Quest for Lower Cabin Altitude," 2024. [Online]. Available: https://bjtonline.com/business-jet-news/flying/the-quest-for-lower-cabin-altitude.

[34] SAFT, "ATR regional airliners upgrade to Saft ULM® batteries for reduced maintenance costs," SAFT, 17 6 2017. [Online]. Available: https://saft.com/en/media-resources/press-releases/atr-regional-airliners-upgrade-saft-ulm%C2%AE-batteries-reduced#:~:text=It%20is%20the%20world%20leader,the%20South%20West%20of%20France.

[35] A. Kundu, "Aircraft Design," Cambridge University Press, Cambridge, 2010.

[36] L. Loftin, "Subsonic Aircraft: Evolution and the Matching of Size Performance," NASA reference Publication 1060, Virginia, 1980.

[37] E. Torenbeek, Synthesis of Subsonic Airplane Design, Delft: Delft Univeristy Press, 1988.

[38] . S. Gudmundsson, General Aviation Aircraft Design: Applied Methods and Procedures, Elsevier: Butterworth-Heinemann, 2014.

[39] Loftin, "Subsonic aircraft: Evolution and the matching of size to performance," NASA, 1980.

[40] D. Chinn and J. Dimson, "A different lens on Europe's defense budgets," *McKinsey & Company,* pp. 1-4, 12 February 2025.

[41] "DLR," 27 January 2022. [Online]. Available: https://www.dlr.de/en/ae/latest/technical-articles/technical-article-2022/no-more-vibrations-viscoelastic-damping-design-for-the-reduction-of-aircraft-vibrations-with-elastomers. [Accessed July 2025].

[42] Z. L. &. Z. L. Zehua-Lied, "Comparison of Emission Properties of Sustainable Aviation Fuels and Conventional Aviation Fuels: A Review," MDPI, Basel, 2024.

[43] L. S. B. O. Voth V, " Estimating Aircraft Power Requirements: A Study of Electrical Power Demand Across Various Aircraft Models and Flight Phases," *Aerospace,* vol. 11(12), 2024.

[44] Cox & Company, "Low Power Ice Protection Systems," Cox & Company, [Online]. Available: https://www.coxandco.com/low_power_ips.html.

[45] ATR, "ATR 72-600," [Online]. Available: https://www.atr-aircraft.com/wp-content/uploads/2020/07/Factsheets_-_ATR_72-600.pdf.

[46] S. Duivenvoorden, "Aerodynamic Interaction Effects Between a Propeller Slipstream and Single Slotted Flap," Delft University of Technology, 2025.

[47] D. P.-B. &. B. Planès, "Modeling and Design Optimization of an Electric Environmental Control System for Commercial Passenger Aircraft," aerospace, Toulouse, 2023.

[48] A. Media, "https://www.allsafe-media.com/fileadmin/user_upload/pdf/Aero/Pax_Seat_Fittings_S022-027_0320.pdf," [Online].

[49] D. U. o. Technology, "Experimental Investigation of Aerodynamic Interactions of a Wing with Deployed Fowler Flap under Influence of a Propeller Slipstream".

[50] Y. G. Z. Yang, "Power optimization of the environmental control system for the civil more electric aircraft".

[51] P. a. Whitney, "Deutsche Aircraft and RTX's Pratt & Whitney Canada collaborate on ensuring 100% SAF readiness for the D328eco™," [Online]. Available: https://www.prattwhitney.com/en/newsroom/news/2024/11/04/deutsche-aircraft-and-rtxs-pratt-whitney-canada-collaborate-on-100-percent-saf-for-d328eco.

[52] F. C. A. D. Luca, "Investigation on the static and dynamic structural behaviors of a regional aircraft main landing gear by a new numerical methodology".